

ARTICLE

centrocortin RNA localization to centrosomes is regulated by FMRP and facilitates error-free mitosis

Pearl V. Ryder*¹, Junnan Fang*¹, and Dorothy A. Lerit¹

Centrosomes are microtubule-organizing centers required for error-free mitosis and embryonic development. The microtubule-nucleating activity of centrosomes is conferred by the pericentriolar material (PCM), a composite of numerous proteins subject to cell cycle-dependent oscillations in levels and organization. In diverse cell types, mRNAs localize to centrosomes and may contribute to changes in PCM abundance. Here, we investigate the regulation of mRNA localization to centrosomes in the rapidly cycling *Drosophila melanogaster* embryo. We find that RNA localization to centrosomes is regulated during the cell cycle and developmentally. We identify a novel role for the fragile-X mental retardation protein in the posttranscriptional regulation of a model centrosomal mRNA, *centrocortin* (*cen*). Further, mistargeting *cen* mRNA is sufficient to alter cognate protein localization to centrosomes and impair spindle morphogenesis and genome stability.

Introduction

The centrosome is a multifunctional organelle that serves as the primary microtubule-organizing center of most animal cells and comprises a central pair of centrioles surrounded by a proteinaceous matrix of pericentriolar material (PCM; Conduit et al., 2015). During mitosis, centrosomes help organize the bipolar mitotic spindle and function to ensure the fidelity of cell division. In interphase, centrosomes contribute to cell polarization, intracellular trafficking, and ciliogenesis (Vertii et al., 2016).

Cell cycle-dependent changes in PCM composition contribute to functional changes in centrosome activity. Upon mitotic entry, centrosomes undergo mitotic maturation, a process by which centrosomes augment their microtubule-nucleating capacity through the recruitment of additional PCM (Palazzo et al., 2000). This process is reversed upon mitotic exit by PCM shedding (Magescas et al., 2019; Mittasch et al., 2020). These dynamic oscillations in PCM composition and organization are essential for centrosome function, and their deregulation is associated with developmental disorders, increased genomic instability, and cancer (Conduit et al., 2015; Nigg and Raff, 2009). Nonetheless, the regulation of PCM dynamics remains incompletely understood.

Centrosomes are essential for early *Drosophila* embryogenesis, which proceeds through 14 rounds of rapid, synchronous, abridged nuclear cycles (NCs) consisting of S and M phases with no intervening gap phases before cellularization (Foe and Alberts, 1983). From NC 10 to 14, the embryo develops as a syncytial blastoderm, wherein thousands of nuclei and their

associated centrosome pairs divide just under the embryonic cortex. Nuclear migration and divisions are coordinated by the centrosomes, and mutations in centrosome-associated genes impair spindle morphogenesis, mitotic synchrony, genome stability, and embryonic viability (Glover et al., 1995; Megraw et al., 1999; Sunkel and Glover, 1988). As in many organisms, the early development of the *Drosophila* embryo proceeds through a period of transcriptional quiescence and is supported by a maternal supply of mRNA and proteins (Vastenhouw et al., 2019). Thus, PCM dynamics apparent in early embryos rely on posttranscriptional mechanisms.

More than a decade ago, a high-throughput screen for mRNAs with distinct subcellular locations in syncytial *Drosophila* embryos uncovered a subset of mRNAs localizing to spindle poles (Lécuyer et al., 2007). Many of the centrosome-enriched transcripts identified in that screen encode known centrosome regulators, including *cyclin B* (*cyc B*) and *pericentrin-like protein* (*plp*; Dalby and Glover, 1992; Martinez-Campos et al., 2004; Raff et al., 1990). These findings raise the possibility that RNA localization, translational control, and other posttranscriptional regulatory mechanisms contribute to centrosome activity and/or function. Consistent with this idea, RNA is known to associate with centrosomes in diverse cell types, including early embryos (*Drosophila*, *Xenopus*, zebrafish, and mollusk), surf clams, and cultured mammalian cells (Alliegro and Alliegro, 2008; Alliegro et al., 2006; Bergalet et al., 2020; Blower et al., 2007; Lambert and Nagy, 2002; Lécuyer et al., 2007; Raff et al.,

Department of Cell Biology, Emory University School of Medicine, Atlanta, GA.

*P.V. Ryder and J. Fang contributed equally to this paper; Correspondence to Dorothy A. Lerit: dlerit@emory.edu.

© 2020 Ryder et al. This article is distributed under the terms of an Attribution-Noncommercial-Share Alike-No Mirror Sites license for the first six months after the publication date (see <http://www.rupress.org/terms/>). After six months it is available under a Creative Commons License (Attribution-Noncommercial-Share Alike 4.0 International license, as described at <https://creativecommons.org/licenses/by-nc-sa/4.0/>).

1990; Sepulveda et al., 2018). The functional consequences and the mechanisms that regulate centrosome-localized RNA remain little understood, however (Marshall and Rosenbaum, 2000; Ryder and Lerit, 2018).

Here, we report that multiple RNAs dynamically localize to centrosomes in *Drosophila* early embryos. We show that these RNAs localize in unique patterns, with some forming higher-order granules and others localizing to centrosomes as individual molecules. We further demonstrate that some RNAs localize to centrosomal subdomains, e.g., centrosome flares, which extend from interphase centrosomes and define the PCM scaffold (Lerit et al., 2015; Megraw et al., 2002; Richens et al., 2015). We identify one centrosomal RNA, *centrocortin* (*cen*), which forms micrometer-scale granules that localize asymmetrically to centrosomes. We further define the mechanisms underlying *cen* mRNA granule formation and function. We find that *cen* mRNA granules include Cen protein and the translational regulator fragile-X mental retardation protein (FMRP), the orthologue of the fragile X syndrome-related RNA-binding protein encoded by the *Fmr1* gene. Our data show that FMRP regulates both the localization and steady-state levels of *cen* RNA and protein. Moreover, we find that reducing *cen* dosage is sufficient to ameliorate mitotic spindle defects associated with *Fmr1* loss. Finally, we show that mislocalization of *cen* mRNA prevents the localization of Cen protein to distal centrosomes and is associated with disrupted embryonic nuclear divisions.

Results

Quantitative analysis of mRNA distributions to *Drosophila* centrosomes

A genome-wide screen identified a cohort of mRNAs showing localization near spindle poles (Lécuyer et al., 2007). To quantitatively assess transcript localization to centrosomes, we combined single-molecule FISH (smFISH) with direct visualization of centrosomes. smFISH permits precise subcellular localization of individual RNA molecules, an important feature when determining enrichment at a relatively small target, such as the centrosome (Raj et al., 2008). For this analysis, we focused on NC 13 embryos, as their prolonged interphase facilitates the collection of sufficient samples for quantification (Foe and Alberts, 1983). We used GFP-Centrosomin (GFP-Cnn) expressed under endogenous regulatory elements to label centrosomes (Lerit et al., 2015). Cnn is a core component of the centrosome scaffold required for the organization of the PCM that defines the outer edge of the centrosome (Conduit et al., 2010, 2014; Megraw et al., 1999). Among the candidate RNAs reported to localize near spindle poles (i.e., *Bsg25D*, *cen*, *cyc B*, *plp*, *small ovary* [*sov*], and *partner of inscuteable* [*pins*] mRNAs), we selected five for investigation based on prior data implicating their protein products in centrosome regulation and/or cell division: *cyc B*, *cen*, *plp*, *sov*, and *pins* (Lécuyer et al., 2007).

To examine patterns of RNA localization, we developed an automated custom image analysis pipeline that calculates the distribution of RNA transcripts relative to the distance from the centrosome (Fig. S1 A; Materials and methods). Briefly, smFISH signals and centrosomes were segmented, and the distances

between individual RNA objects and the closest centrosome were measured. This analysis allowed us to calculate the percentage of mRNA overlapping with the centrosome surface (Fig. S1 B, arrowheads).

Several prior studies noted an enrichment of *cyc B* mRNA in the spindle pole region of syncytial *Drosophila* embryos (Dalby and Glover, 1992; Raff et al., 1990; Vardy and Orr-Weaver, 2007). Therefore, we initially investigated the localization of *cyc B* relative to a nonlocalizing control RNA, *gapdh*, to validate our quantitative imaging approach. Consistent with other reports, we observed that *cyc B* was particularly abundant at the posterior pole (Raff et al., 1990). To standardize measurements of mRNA enriched near somatic centrosomes across samples, we imaged embryos at ~50% egg length unless otherwise noted. To monitor cell cycle-dependent changes in RNA distribution, centrosome enrichments were calculated during interphase and metaphase. Interphase embryos were selected based on their round nuclei with noncondensed chromosomes and duplicated centrosomes, while metaphase embryos were selected by the presence of a metaphase plate. Throughout the cell cycle, *gapdh* mRNA appeared dispersed throughout the cytoplasm, and <3% overlapped with centrosomes despite high levels of expression (Fig. 1, A–C; Graveley et al., 2011). By contrast, threefold more *cyc B* mRNA overlapped with interphase centrosomes (Fig. 1, D–F; $P < 0.0001$). During metaphase, however, *cyc B* showed less centrosome enrichment than *gapdh*, raising the possibility that *cyc B* mRNA may be actively excluded from mitotic centrosomes (Fig. 1 F; $P < 0.05$). These findings reveal that *cyc B* localization to centrosomes is regulated by cell cycle progression. Moreover, these data showcase the utility of our analysis pipeline to quantitatively define RNA localization to centrosomes.

Multiple mRNAs are enriched at centrosomes in a cell cycle-dependent manner

We next investigated the localization of *plp* mRNA, as PLP protein cooperates with Cnn to mediate centrosome scaffolding (Lerit et al., 2015; Richens et al., 2015). Recently, orthologous PCNT transcripts were shown to be localized to centrosomes in zebrafish embryos and cultured mammalian cells, specifically during early mitosis (Sepulveda et al., 2018). *plp* mRNA was significantly enriched at centrosomes throughout the cell cycle, particularly during interphase, when approximately fourfold more *plp* than *gapdh* mRNA resides at centrosomes (Fig. 1, G–I; $P < 0.0001$). Enrichment of *plp* mRNA is coincident with the formation of interphase centrosome flares containing PLP protein (Lerit et al., 2015), hinting that aspects of *plp* posttranscriptional regulation may be differentially regulated over the cell cycle.

We similarly analyzed the localization of *pins* and *sov* mRNAs to centrosomes. Relative to *gapdh*, significantly more *pins* mRNA localized to interphase centrosomes (Fig. S1, C–E). By contrast, *sov* mRNA was concentrated at centrosomes throughout the cell cycle (~10-fold more than *gapdh*; Fig. S1, F–H). As previously noted, *sov* mRNA tended to localize along centrosome flares (Lécuyer et al., 2007; Fig. S1 F, arrowheads).

Our quantitative analysis underscores transcript-dependent and cell cycle stage-dependent variabilities in centrosome

Table 1. Quantification of RNA localization to centrosomes

Genotype	mRNA	NC stage	Cell cycle phase	Embryos (n)	Centrosomes (n)	mRNA objects (n)
GFP-Cnn	<i>cen</i>	NC 10	Interphase	20	291	165,767
GFP-Cnn	<i>cen</i>	NC 10	Metaphase	17	272	95,665
GFP-Cnn	<i>cen</i>	NC 13	Interphase	18	3,048	118,306
GFP-Cnn	<i>cen</i>	NC 13	Metaphase	17	2,169	162,043
GFP-Cnn	<i>cyc B</i>	NC 13	Interphase	19	3,247	177,536
GFP-Cnn	<i>cyc B</i>	NC 13	Metaphase	13	1,667	143,962
GFP-Cnn	<i>gapdh</i>	NC 10	Interphase	19	298	248,645
GFP-Cnn	<i>gapdh</i>	NC 10	Metaphase	18	298	209,717
GFP-Cnn	<i>gapdh</i>	NC 13	Interphase	16	2,362	112,165
GFP-Cnn	<i>gapdh</i>	NC 13	Metaphase	16	2,096	76,762
GFP-Cnn	<i>pins</i>	NC 13	Interphase	24	3,642	117,132
GFP-Cnn	<i>pins</i>	NC 13	Metaphase	15	1,911	74,495
GFP-Cnn	<i>plp</i>	NC 13	Interphase	19	2,899	27,476
GFP-Cnn	<i>plp</i>	NC 13	Metaphase	17	2,392	27,542
GFP-Cnn	<i>sov</i>	NC 13	Interphase	19	3,689	81,150
GFP-Cnn	<i>sov</i>	NC 13	Metaphase	17	1,960	46,055
GFP- γ -Tub	<i>cen</i>	NC 10	Interphase	13	192	122,555
GFP- γ -Tub	<i>cen</i>	NC 10	Metaphase	10	220	86,483
GFP- γ -Tub; <i>Fmr1</i>	<i>cen</i>	NC 10	Interphase	12	192	100,816
GFP- γ -Tub; <i>Fmr1</i>	<i>cen</i>	NC 10	Metaphase	12	205	56,786
GFP- γ -Tub	<i>cen</i>	NC 13	Interphase	27	3,458	192,394
GFP- γ -Tub	<i>cen</i>	NC 13	Metaphase	12	1,228	67,961
GFP- γ -Tub; <i>Fmr1</i>	<i>cen</i>	NC 13	Interphase	27	3,088	142,762
GFP- γ -Tub; <i>Fmr1</i>	<i>cen</i>	NC 13	Metaphase	12	1,222	46,690

enrichment, suggesting that RNA localization to centrosomes is a regulated process, often favoring localization to interphase centrosomes. Differential mRNA localization over the cell cycle also implies that RNA localization to centrosomes is likely to be a dynamic process.

Dynamic regulation of micrometer-scale *cen* mRNA granules

We next investigated the localization of *cen* mRNA. *Cen* was previously shown to be required for normal nuclear divisions in *Drosophila* embryos (Kao and Megraw, 2009). Moreover, *cen* mRNA was recently localized to embryonic centrosomes (Bergalet et al., 2020). Unlike the other transcripts we investigated, the majority of *cen* mRNA was enriched at centrosomes during interphase (Fig. 2 A, arrow). *cen* mRNA displayed a propensity to form higher-order structures, or RNA granules, defined as an overlapping cluster of four or more mRNAs (Little et al., 2015). Throughout NC 13, *cen* mRNA formed micrometer-scale granules, consistent with recent work (Fig. 2, A and B, arrows and arrowheads; Bergalet et al., 2020). Demonstrating specificity, these signals were not detected in null *cen* embryos (Fig. 2 C). Quantification revealed that nearly 60% of *cen* mRNA overlapped with interphase centrosomes (Fig. 2 D). Although this enrichment declined to ~25% during metaphase, *cen* mRNA

remained significantly enriched at centrosomes relative to *gapdh* (Fig. 2 D). The majority of *cen* mRNA resided in granules, which showed a biased localization to the mother centrosome during interphase (Fig. 2, A, E, and F, arrow). During metaphase, *cen* mRNA granules appeared less tightly associated with centrosomes (Fig. 2, B and F, arrowhead). We conclude that *cen* mRNA organizes into pericentrosomal granules in a cell cycle-dependent manner, resulting in a bulk enrichment of *cen* mRNA at centrosomes.

The strong enrichment of *cen* mRNA within pericentrosomal granules prompted us to investigate the timing of their formation. In interphase NC 10 embryos, *cen* mRNA predominantly existed in single molecules radiating in a gradient from centrosomes (Fig. 2 G). Entry into mitosis correlated with formation of *cen* mRNA granules that were closely apposed and symmetrically distributed to the two centrosomes (Fig. 2 H). Throughout NC 10, significantly more *cen* mRNA than *gapdh* was found at centrosomes (Fig. 2 I). Similarly, significantly more *cen* mRNA than *gapdh* was contained within granules, particularly during metaphase (>100-fold difference; Fig. 2 J). These data suggest that the formation of *cen* mRNA granules is entrained with the cell cycle and correlates with the initiation of cortical nuclear divisions. Our finding that *cen* mRNA persists in RNA granules

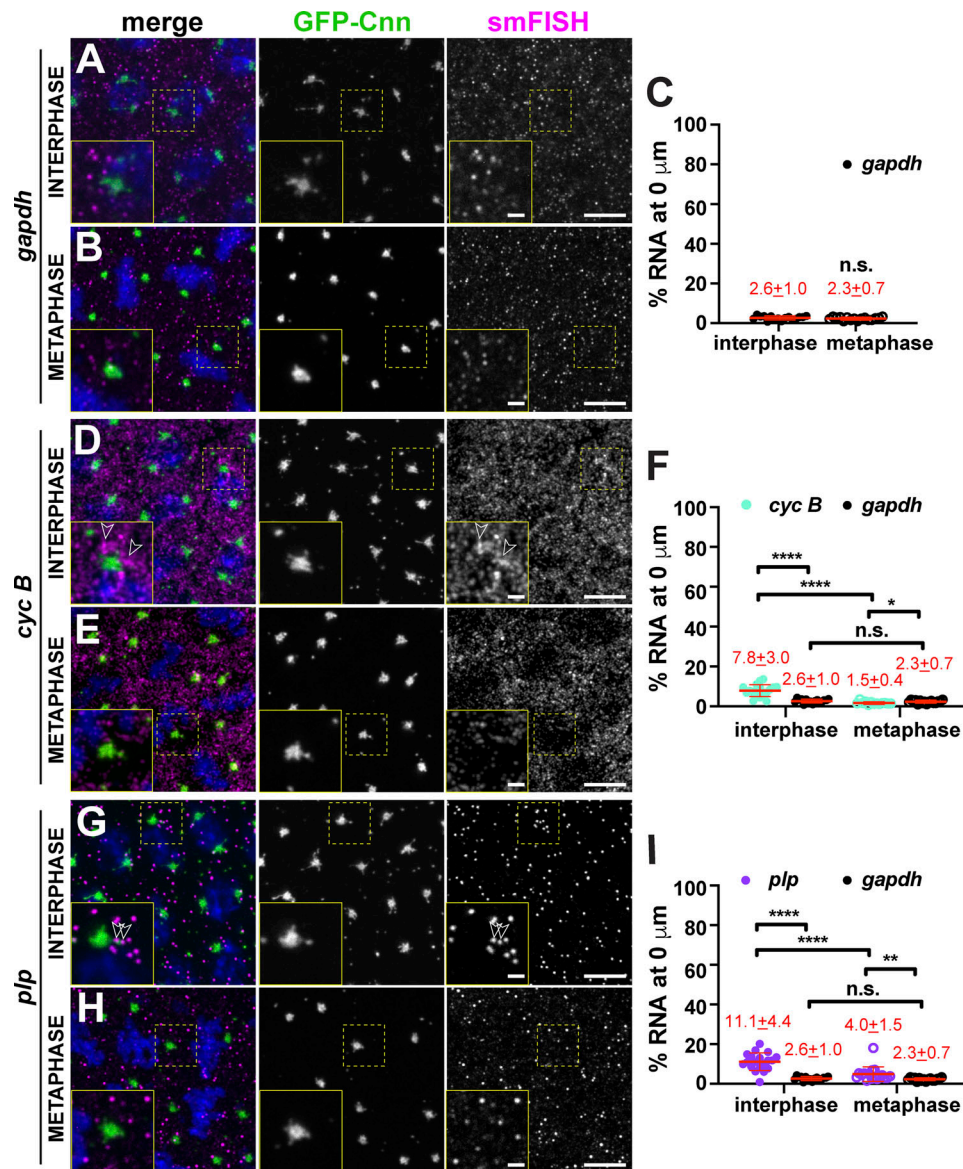


Figure 1. **Quantitative localization of mRNA to centrosomes.** Maximum-intensity projections of smFISH (magenta) in NC 13 embryos expressing the centrosome marker GFP-Cnn (green). DAPI labels nuclei blue. Boxed regions enlarged in insets. Open arrowheads mark mRNA at the PCM. Quantification of the percentage of RNA overlapping with the centrosome surface ($0\ \mu\text{m}$ distance) is shown to the right, where each dot represents a single measurement from $n = 16$ interphase and metaphase (*gapdh* mRNA), 19 interphase and 13 metaphase (*cyc B* mRNA), and 19 interphase and 17 metaphase (*plp* mRNA) embryos, respectively. Mean \pm SD displayed (red). (A–I) *gapdh* (A–C), *cyc B* (D–F), and *plp* mRNAs (G–I). Note that values for *gapdh* are reproduced from C for comparison. Table 1 lists the number of embryos, centrosomes, and RNA objects quantified per condition. *, $P < 0.05$; **, $P < 0.01$; ****, $P < 0.0001$ by ANOVA followed by Dunnett’s T3 multiple comparisons test. Scale bars: $5\ \mu\text{m}$; $1\ \mu\text{m}$ (insets). n.s., not significant.

in interphase NC 13 embryos suggests that the capacity for *cen* mRNA granule formation or maintenance is additionally regulated developmentally.

The *cen* mRNA granule contains Cen protein and requires the centrosome scaffold

To gain insight into the regulation and function of *cen* mRNA granules, we first investigated their composition. Recent work uncovered that *cen* mRNA granules contain Cen protein, and some *cen* mRNA granules represent sites of local translation (Bergalet et al., 2020). We similarly noted a strong coincidence of *cen* mRNA and protein at centrosomes, confirming that Cen

protein is abundant in *cen* mRNA granules (Fig. 3, A and B, arrows).

Cen interacts directly with the centrosome scaffold protein Cnn, and a point mutation in Cnn, *cnn^{B4}*, is sufficient to disrupt Cen–Cnn binding and, consequently, Cen protein localization to centrosomes (Kao and Megraw, 2009). To test whether the centrosome scaffold is required for RNA localization, we examined if *cen* mRNA localized to pericentrosomal granules in *cnn^{B4}* mutants. We found that *cen* mRNA no longer formed granules in *cnn^{B4}* embryos and instead appeared dispersed throughout the cytoplasm (Fig. S2 A). This behavior subsequently allowed us to test if *cen* mRNA granules were required

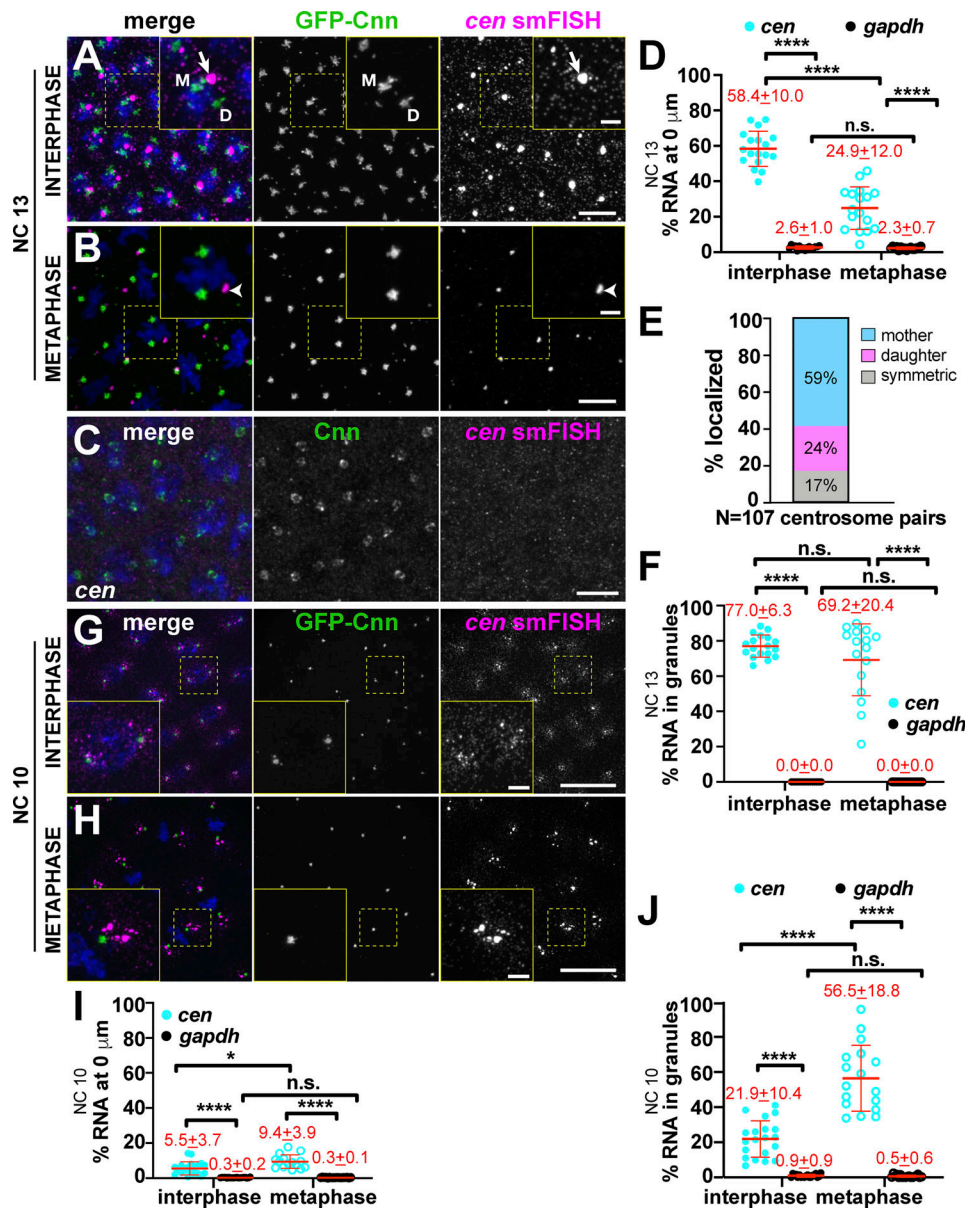


Figure 2. *cen* mRNA localization to centrosomes is cell cycle regulated. Maximum-intensity projections of *cen* smFISH (magenta), where Cnn (green) labels centrosomes. Boxed regions enlarged in insets. **(A)** Interphase NC 13 embryo showing *cen* mRNA granules (arrow). Mother (M) and daughter (D) centrosomes noted. **(B)** Metaphase NC 13 embryo with *cen* mRNA (arrowhead) displaced from centrosomes. **(C)** *cen* mRNA is not detected in *cen* mutants. **(D)** Percentage of RNA overlapping with centrosomes in NC 13. Note that values for *gapdh* are reproduced from Fig. 1 C for comparison. **(E)** Frequency distribution of *cen* mRNA granule localization from $n = 107$ centrosome pairs and $n = 5$ embryos. **(F)** Percentage of *cen* mRNA residing within granules (≥ 4 overlapping RNA molecules) in NC 13. **(G)** Interphase NC 10 embryo with *cen* mRNA symmetrically distributed to centrosomes. **(H)** Metaphase NC 10 embryo with *cen* mRNA granules. **(I)** Percentage of RNA overlapping with centrosomes in NC 10. **(J)** Percentage of *cen* mRNA within granules in NC 10. Each dot represents a measurement from a single embryo. Mean \pm SD displayed (red) from $n = 16$ interphase and metaphase (*gapdh* mRNA), 18 interphase and 17 metaphase (*cen* mRNA) NC 13; $n = 19$ interphase and 18 metaphase (*gapdh* mRNA); and 20 interphase and 17 metaphase (*cen* mRNA) NC 10 embryos, respectively. Table 1 lists number of objects quantified per condition. *, $P < 0.05$; ****, $P < 0.0001$ by ANOVA followed by Dunnett's T3 multiple comparisons test (D, I, and J) and the Kruskal-Wallis test followed by Dunn's multiple comparisons test (F). Scale bars: 10 μm ; 2.5 μm (insets). n.s., not significant.

for Cen translation. We observed no difference in the levels of Cen protein in WT versus *cnm*^{B4} mutant 0–2-h embryos (Fig. S2, B and B'). These data suggest that the *cen* mRNA granule is not required for normal steady-state levels of Cen protein; however, an important caveat is that maternal deposition of Cen may obscure changes resulting from granule loss. Nonetheless, our data support a model in which the centrosome scaffold

contributes to the formation and/or localization of the *cen* mRNA granule, likely via associations between Cen and Cnn.

FMRP associates with *cen* granules

RNA granules are diverse structures, and RNA-binding proteins are crucial for their formation and function (Singh et al., 2015). Therefore, to provide mechanistic insight into the regulation of

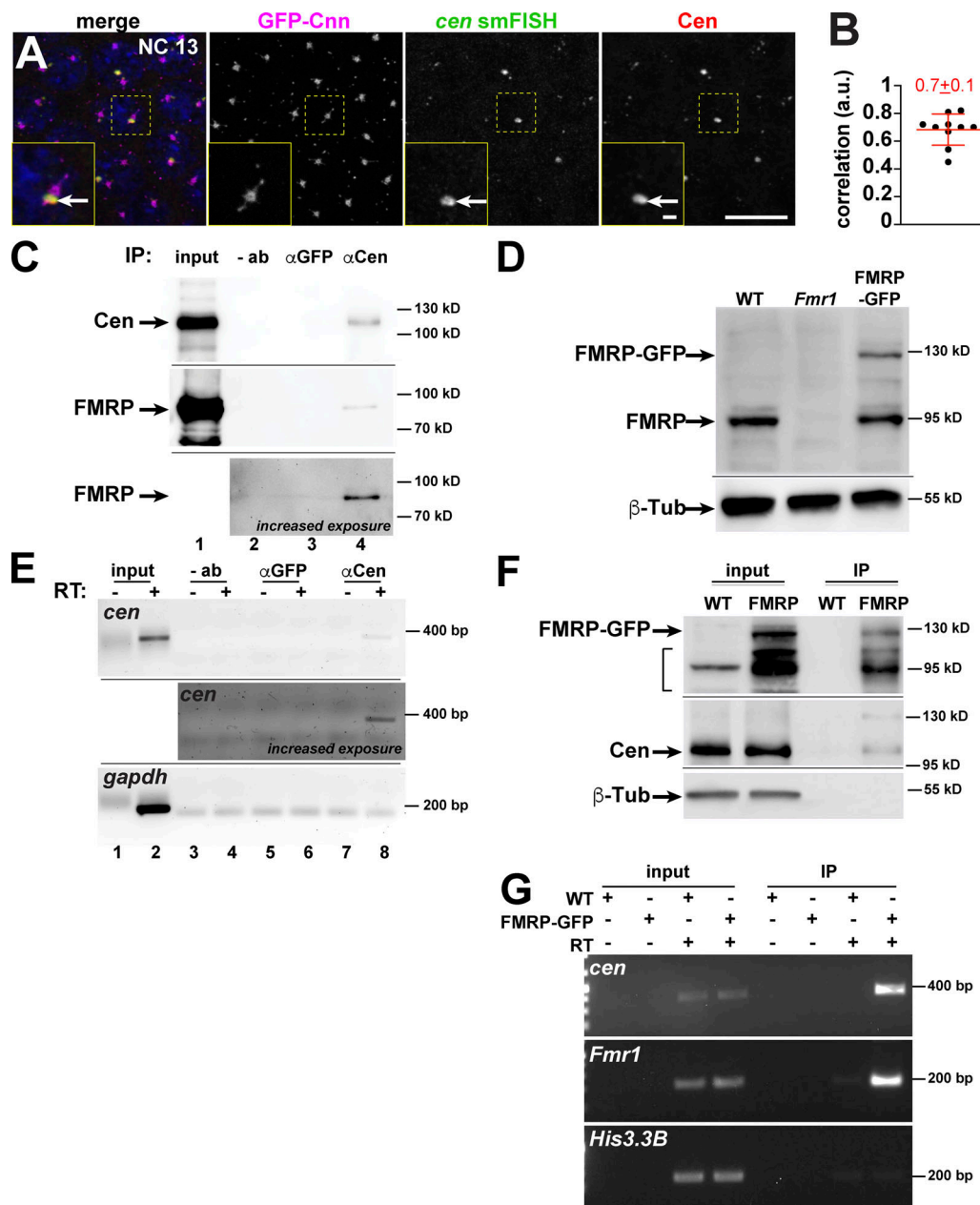


Figure 3. Composition of the *cen* mRNA granule. (A) Maximum-intensity projection of a NC 13 embryo expressing GFP-Cnn (magenta) showing colocalization of *cen* mRNA (green) and protein (red). Boxed region enlarged in insets; arrows, *cen* mRNA granule. (B) Pearson's correlation coefficient for *cen* smFISH and Cen signals. Each dot is a single measurement from $n = 10$ NC 13 embryos; mean \pm SD displayed (red). (C) Blots from Cen immunoprecipitation (IP) using 1–3-h (~NC 7–14) embryo extracts. Lane 1, 10% input; lane 2, empty beads; lane 3, rabbit anti-GFP antibody; and lane 4, rabbit anti-Cen antibody. Cen pulls down itself (top) and FMRP (middle and bottom). Lower blot shows increased exposure to highlight FMRP, with lane 1 cropped due to oversaturated signal. (D) Blot shows FMRP levels in 0–2-h (up to NC 14) embryos of the indicated genotypes using anti-FMRP antibody. (E) RNA-immunoprecipitation where RT-PCR reactions were run in the presence (+) or absence (-) of reverse transcriptase (RT). Lanes 1 and 2, 10% input; lanes 3 and 4, empty beads; lanes 5 and 6, rabbit anti-GFP antibody; and lanes 7 and 8, rabbit anti-Cen antibody. Middle image shows increased exposure to highlight *cen*; note that lanes 1 and 2 were cropped owing to oversaturated signal. (F) Blots from FMRP-GFP immunoprecipitation using 0–2-h WT or FMRP-GFP (FMRP) embryonic extracts and GFP-Trap beads probed with rabbit anti-GFP (top), rabbit anti-Cen (middle), and mouse anti- β -Tub antibodies (bottom). GFP pulls out FMRP-GFP and Cen protein. Bracket denotes nonspecific and/or degradation products. (G) RNA-immunoprecipitation from GFP-Trap beads, where *Fmr1* (positive control; Ling et al., 2004) and *cen* mRNAs are pulled down (last lane), while *His3.3B* mRNA (negative control) is not. Full gels/blots available on FigShare (see Materials and methods). Scale bars: 10 μ m; 1 μ m (insets). a.u., arbitrary units.

the *cen* mRNA granule, we assayed the centrosomal localization of a few candidate RNA-binding proteins, including maternal expression at 31B (me31B), Pumilio (Pum), Egalitarian (Egl), Orb2, and FMRP (Deshpande et al., 2006; Dienstbier et al.,

2009; Gamberi et al., 2006; Fig. S2, C–G'). Among these, FMRP appeared to be cytoplasmic, with a subset of puncta overlapping with centrosomes (Fig. S2 G', arrowheads). We selected FMRP for further analysis.

To further investigate the composition of *cen* mRNA granules, we probed for biochemical interactions. We isolated endogenous Cen protein complexes from embryos by immunoprecipitation and detected a specific association with FMRP (Fig. 3 C). Specificity of the FMRP antibody was validated by immunoblot (Fig. 3 D). We similarly coisolated *cen* mRNA, but not the control *gapdh*, from Cen pull-downs (Fig. 3 E). The interaction between Cen and FMRP was confirmed by using a construct that expresses FMRP-GFP under endogenous regulatory elements (Sudhakaran et al., 2014) and reversing the direction of immunoprecipitation. Immunoblotting confirmed that FMRP-GFP was not overexpressed relative to endogenous FMRP levels (Fig. 3 D). Using GFP-Trap beads, we isolated FMRP protein and detected a specific association with Cen (Fig. 3 F). FMRP associates with *Fmr1* mRNA (Ling et al., 2004). We confirmed this interaction and also detected a specific interaction between FMRP and *cen* mRNA, but not the control *Histone H3.3B* (*His3.3B*; Fig. 3 G). Therefore, the *cen* mRNA granule represents a ribonucleoprotein (RNP) complex comprising *cen* mRNA, Cen, FMRP, and likely other constituents. These data also hint that FMRP may mediate aspects of *cen* mRNA regulation.

FMRP functions as a negative regulator of *cen* mRNA granule formation and localization to centrosomes

FMRP is a multifunctional RNA-binding protein implicated in RNA localization, stability, and translational regulation (Banerjee et al., 2018). To determine if FMRP contributes to *cen* regulation, we first compared the localization of *cen* mRNA in WT versus *Fmr1* null mutant embryos expressing the PCM marker GFP- γ -Tubulin (GFP- γ -Tub). In WT NC 10 interphase embryos, *cen* mRNA was predominantly distributed as single molecules enriched near centrosomes, as we previously noted (Fig. 2 G; Fig. 4 A and inset). In *Fmr1* embryos, however, significantly more *cen* mRNA clustered near centrosomes (Fig. 4, B–D). Quantification confirmed that *cen* mRNA localization to centrosomes and residence within RNA granules were both significantly higher in *Fmr1* embryos relative to WT (Fig. 4, E and F). These data suggest that FMRP regulates *cen* mRNA granule formation and localization to centrosomes.

We noted similar trends later in development, during NC 13, when significantly more *cen* mRNA distributed to pericentrosomal granules in *Fmr1* embryos than WT (Fig. 5, A–D). Quantification highlighted a significant enrichment of *cen* mRNA at centrosomes and within RNA granules in *Fmr1* embryos relative to WT, particularly during interphase (Fig. 5, E and F), suggesting that FMRP normally limits *cen* mRNA localization to centrosomes. In sum, loss of FMRP is associated with more *cen* mRNA localized to granules, which reside closer to and are more likely to overlap with centrosomes.

FMRP regulates the abundance of *cen* mRNA and protein

The early embryo is largely transcriptionally inactive for the first 2 h of development, and most RNAs are maternally endowed (Anderson and Lengyel, 1979). Thus, the enhanced formation of *cen* mRNA granules in *Fmr1* mutants could be attributed to changes in mRNA localization, increased mRNA stability, or both.

To test if FMRP regulates *cen* mRNA levels, we examined normalized *cen* mRNA levels by qPCR. We found no significant change in *cen* mRNA levels in *Fmr1* versus WT 0–1-h embryos, a period encompassing up to NC 7 ($P = 0.07$ by unpaired *t* test; Fig. 6 A; Foe et al., 1993). FMRP functions primarily as a translational repressor, and deregulation of FMRP targets in neurons is considered a significant driver of fragile X syndrome pathophysiology (Banerjee et al., 2018; Darnell, 2011). In 0–1-h embryos, total levels of Cen protein were unaffected by loss of *Fmr1* ($P = 0.9$ by unpaired *t* test; Fig. 6, B and B'). In contrast, within 1–3-h embryos (~NC 7–14), *cen* mRNA levels increased 1.8-fold in *Fmr1* mutants relative to controls ($P < 0.0001$ by unpaired *t* test; Fig. 6 C), and *Fmr1* embryos contained significantly more Cen protein than controls (3.7-fold increase relative to WT, $P = 0.03$ by unpaired *t* test; Fig. 6, D and D'). Thus, both *cen* mRNA and protein levels are increased in later-stage *Fmr1* embryos. Taken together, these data suggest that FMRP may contribute to *cen* mRNA turnover and/or translational repression. Although *cen* mRNA localization and levels may be coupled, such that increased *cen* mRNA content accounts for augmented *cen* mRNA localization to centrosomes and translation in *Fmr1* mutants, we cannot rule out the possibility that FMRP contributes to multiple aspects of *cen* mRNA posttranscriptional regulation, either directly or indirectly.

cen and FMRP functionally interact to regulate cell division and embryonic viability

FMRP has established roles in mitotic progression. In *Drosophila* embryos, loss of FMRP results in severe mitotic defects, including improper centrosome separation, loss of mitotic synchrony, and faulty cellularization (Deshpande et al., 2006; Monzo et al., 2006; Papoulas et al., 2010; Sullivan et al., 1993). Using hatch rate analysis as a measure of embryonic viability, we found that while *Fmr1* mutants show an average of 6.3% unhatched embryos, *cen* hemizygoty partially restored viability ($P < 0.05$ vs. *Fmr1* by unpaired *t* test; Fig. 6 E). Western blot analysis confirmed that *cen* hemizygoty normalized Cen protein levels in *Fmr1* embryos (Fig. 6, F and F'). These data are consistent with a genetic interaction between *cen* and *Fmr1*; moreover, they implicate elevated Cen dosage as a driver of *Fmr1*-mediated embryonic lethality.

To test if *cen* genetically modifies the mitotic defects observed in *Fmr1* mutant embryos, we tabulated the incidence of abnormal microtubule spindles, including bent, multipolar, monopolar, or fused spindles (Materials and methods). Occasionally, even WT embryos contained aberrant microtubule spindles (3.7%, $n = 1/27$ embryos; Fig. 7, A and E). However, *cen* mutant embryos showed increased rates of spindle errors (40.9%, $n = 9/22$ embryos, $P < 0.01$ vs. WT; Fig. 7, B and E, arrowheads), in agreement with prior observations (Bergalet et al., 2020; Kao and Megraw, 2009). Similarly, loss of *Fmr1* was associated with high rates of spindle defects (76.1%, $n = 23/30$ embryos, $P < 0.0001$ cf. WT; Fig. 7, C and E, arrows). Consistent with this result, areas of reduced nuclear density (i.e., nuclear fallout) were noted in *Fmr1* embryos (Fig. 7 C, dashed lines). Reducing *cen* dosage, however, ameliorated the spindle defects in *Fmr1* mutants (48.1%, $n = 13/27$ embryos, $P < 0.05$; Fig. 7, D and E). Together, these data

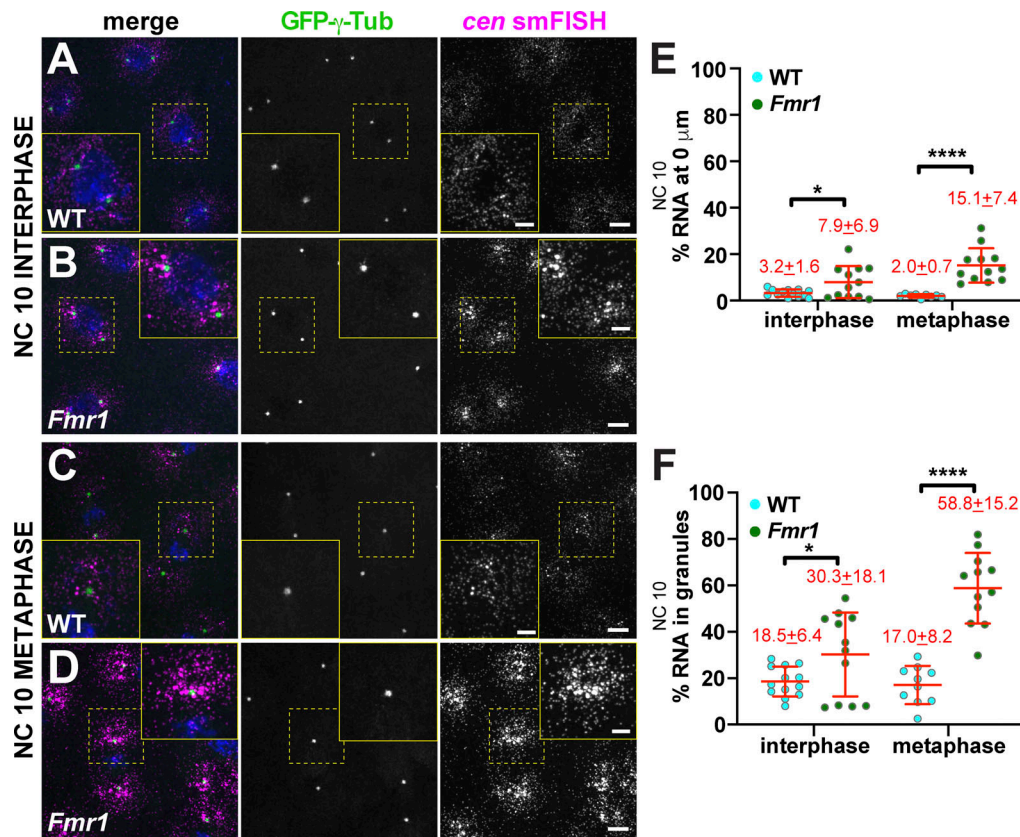


Figure 4. ***Fmr1* regulates *cen* mRNA granule formation.** Maximum-intensity projections of *cen* smFISH (magenta) in NC 10 embryos expressing GFP- γ -Tub (green). Boxed regions are enlarged at right (yellow box, zoom). (A) WT NC 10 interphase embryo with *cen* mRNA at centrosomes. (B) *Fmr1* embryo with more granular, pericentrosomal *cen* mRNA. (C) WT NC 10 metaphase embryo. (D) *Fmr1* embryo showing increased *cen* mRNA at centrosomes. (E) Percentage of *cen* mRNA overlapping with centrosomes in WT versus *Fmr1* embryos. (F) Percentage of *cen* mRNA within granules. Each dot is a single measurement from $n = 13$ interphase and 10 metaphase WT and $n = 12$ interphase and metaphase *Fmr1* embryos. Mean \pm SD displayed (red). Table 1 lists number of objects quantified per condition. *, $P < 0.05$; ****, $P < 0.0001$ by unpaired t test. Scale bars: 10 μ m; 2.5 μ m (insets).

demonstrate that normal *cen* dosage is required for spindle morphogenesis and that the up-regulation of *cen* in *Fmr1* embryos contributes to an increased rate of spindle errors and embryonic lethality.

Ectopic *cen* mRNA localization disrupts mitosis

Our data support a model whereby the local concentration of *cen* mRNA contributes to proper cell cycle progression. To test this model, we engineered a chimeric RNA comprising the *cen* coding sequence and the *bicoid* (*bcd*) 3'UTR, previously shown to be sufficient to mislocalize target RNAs to the anterior pole (Macdonald and Struhl, 1988). For these experiments, we examined embryos from mothers expressing the *cen-bcd-3'UTR* transgene in the context of the *cen* null background (hereafter, *cen-bcd-3'UTR* embryos).

We first confirmed that our transgenic construct successfully mistargeted *cen* mRNA to the anterior. *cen-bcd-3'UTR* embryos showed a crescent of *cen* mRNA and protein at the anterior pole (Fig. 8, A and B). Immunoblotting showed that Cen protein is overexpressed in *cen-bcd-3'UTR* embryos, similar to *Fmr1* mutants (approximately threefold increase vs. WT, $P < 0.05$ by unpaired t test; Fig. 8, C and C'). Given its restricted localization to the anterior pole, the *cen-bcd-3'UTR* transgene allowed us to

simultaneously test opposing effects of *cen* dosage. We examined the effect of excess *cen* by visualizing the anterior pole, and we examined the effect of local *cen* mRNA depletion by visualizing the embryo midregion.

At the anterior of *cen-bcd-3'UTR* embryos, *cen* mRNA and protein coalesced into massive RNPs (Fig. 8 D). Consistent with precocious formation of *cen* mRNA granules, *cen-bcd-3'UTR* RNPs were also prominent during NC 10 (Fig. S3). Through the use of reporter constructs, it was recently demonstrated that the *cen* coding sequence is sufficient for centrosome targeting (Bergalet et al., 2020). In agreement with these data, the enlarged *cen* RNPs observed in *cen-bcd-3'UTR* embryos associated with centrosomes at the anterior pole (Fig. 8 D, dashed circle). Furthermore, we did not observe *cen* mRNA or protein localized to more distal centrosomes in *cen-bcd-3'UTR* embryos, indicating that localization elements within the *bcd-3'UTR* confine *cen* mRNA to the anterior pole. These findings further suggest that localization of *cen* mRNA is necessary and sufficient for Cen protein localization to centrosomes.

The restricted localization of *cen* mRNA and protein to the anterior pole within *cen-bcd-3'UTR* embryos allowed us to test whether *cen* mRNA was required locally for error-free mitosis. Examination of mitotic spindles at $\sim 50\%$ egg length, an area

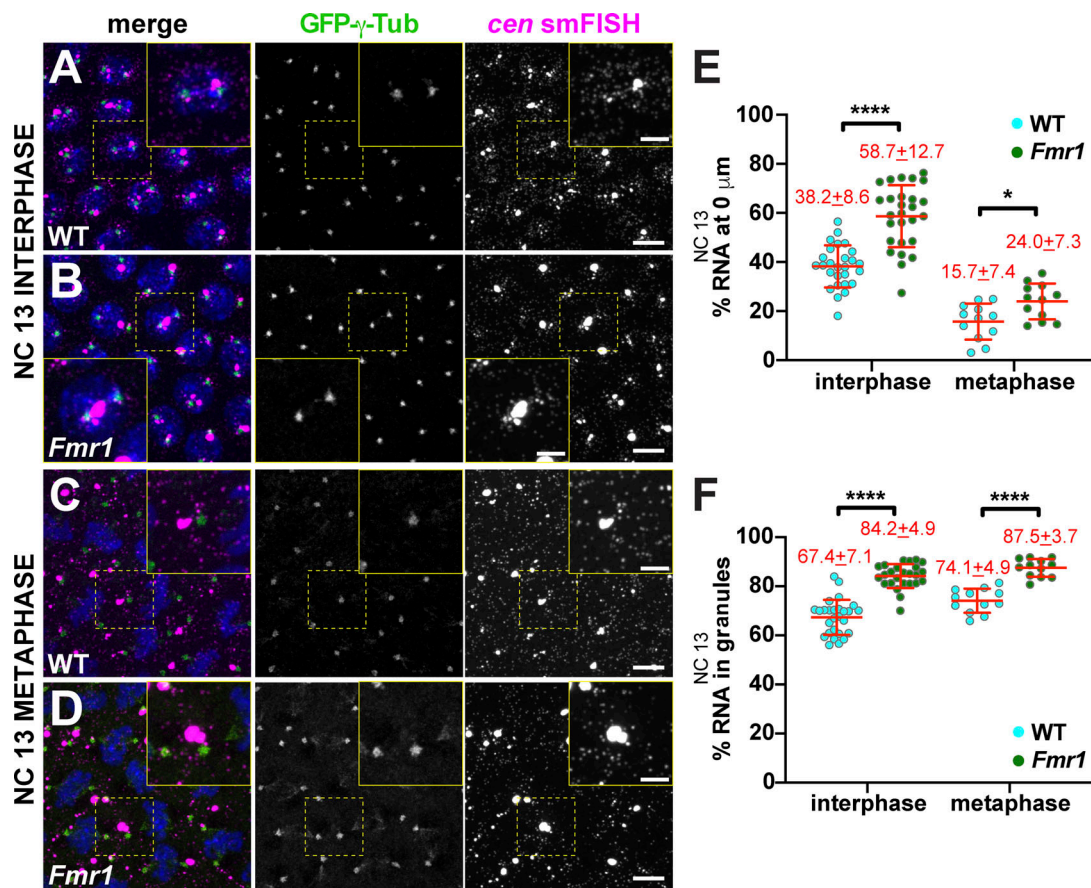


Figure 5. **FMRP regulates *cen* mRNA localization to centrosomes.** Maximum-intensity projections of *cen* smFISH (magenta) in NC 13 embryos expressing GFP- γ -Tub (green). Boxed regions are enlarged at right (yellow box, zoom). (A) WT interphase embryo showing *cen* mRNA granules. (B) *Fmr1* embryo with increased *cen* mRNA in pericentrosomal granules. (C) WT metaphase embryo with *cen* mRNA displaced from the centrosome. (D) *Fmr1* embryo with *cen* mRNA at centrosomes. (E) Percentage of *cen* mRNA overlapping with centrosomes in WT versus *Fmr1* embryos. (F) Percentage of *cen* mRNA within granules. Each dot is a single measurement from $n = 27$ interphase and $n = 12$ metaphase WT or *Fmr1* NC 13 embryos; mean \pm SD displayed (red). Table 1 lists number of objects quantified per condition. *, $P < 0.05$; ****, $P < 0.0001$ by unpaired t test. Scale bars: 10 μ m; 2.5 μ m (insets).

devoid of *cen* mRNA and protein, revealed an increased rate of microtubule spindle defects (47.6%, $n = 10/21$ embryos, $P < 0.001$ vs. WT; Figs. 7 E and 8 E). Together with recent work showing that the native *cen* 3'UTR recruits *I-kappaB* kinase ϵ (*IKK ϵ* or *ik2*) mRNA to centrosomes (Bergalet et al., 2020), these data suggest that *cen* mRNA functions locally to support spindle integrity, perhaps in concert with *ik2* mRNA.

The anterior pole of *cen-bcd-3'UTR* embryos showed lower nuclear density (i.e., nuclear fallout), dysmorphic nuclei, and mitotic asynchrony, indicative of disrupted nuclear divisions (Fig. 8 F). In accordance with these findings, 85% of *cen-bcd-3'UTR* embryos displayed spindle defects at the anterior ($n = 17/20$ embryos, $P < 0.0001$ vs. WT; Fig. 7 E), as well as nuclei associated with supernumerary centrosomes (Fig. 8 D dashed circle). Notably, the large RNPs that form in *cen-bcd-3'UTR* embryos were sufficient to recruit FMRP, as evidenced by a significant overlap of Cen and FMRP signals ($P < 0.01$; Fig. 9, A-C). In addition to overlapping Cen and FMRP signals, we note a concentration of Cen residing at the periphery of the enlarged *cen* RNPs (Fig. 9 B, insets). Given these phenotypes, we next examined embryonic viability. While *cen* mutant embryos show

an elevated rate of unhatched embryos relative to controls, as previously noted (10.7% unhatched; (Kao and Megraw, 2009), *cen-bcd-3'UTR* embryos had increased lethality (mean 19.2%; $P < 0.05$ vs. *cen* by unpaired t test; Fig. 9 D). We propose a model in which the deregulated balance of Cen levels impairs mitotic spindle organization (Fig. 9 E).

Discussion

Centrosome-localized RNA has been described in a variety of organismal contexts, and while the conserved feature of mRNA at centrosomes hints at a biological function, the underlying physiological significance has remained unclear (Marshall and Rosenbaum, 2000; Ryder and Lerit, 2018). To address this question, we systematically examined five transcripts shown to enrich near spindle poles to quantitatively define their common and unique localization patterns in *Drosophila* embryos. We identified subsets of mRNAs showing centrosome enrichment in a cell cycle-regulated and developmentally regulated manner. These nonrandom variances in RNA distributions further imply biological relevance. We tested if RNA localization contributes

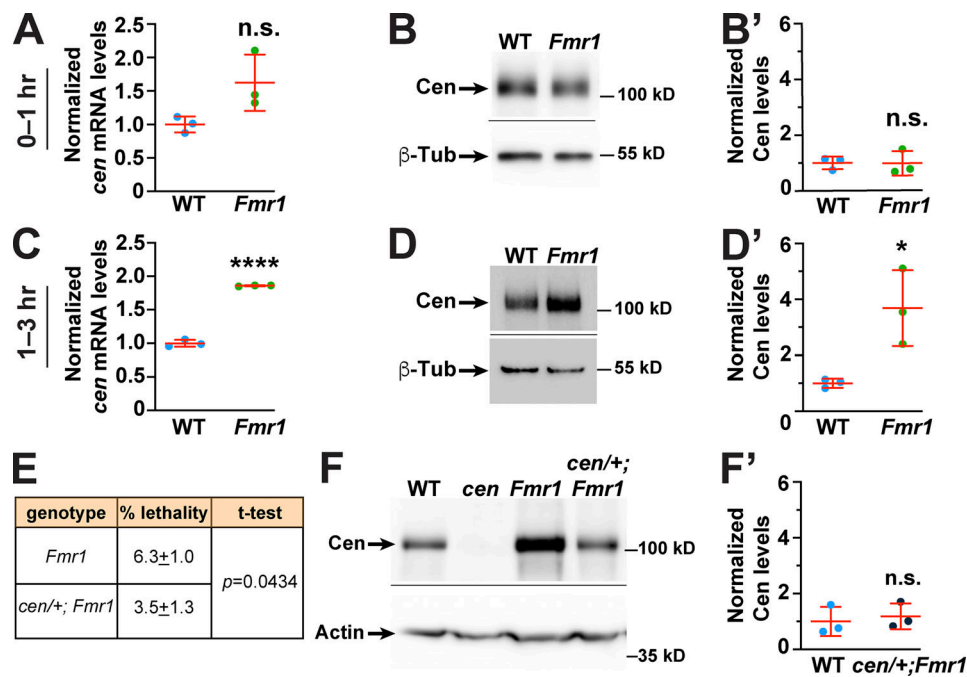


Figure 6. **FMRP regulates levels of *cen* mRNA and protein levels.** (A) Levels of *cen* RNA were normalized to *RP49* as detected by qPCR from 0- to 1-h (up to NC 7) embryos. (B) Blots show Cen protein levels relative to the β-Tub loading control from 0-1-h embryos and quantified in B'. (C) Normalized levels of *cen* RNA from 1-3-h (~NC 7-NC 14) embryos. (D) Blots show Cen protein in 1-3-h embryos and quantified in D'. (E) Embryonic lethality rates in *Fmr1* versus *cen/+; Fmr1* embryos. The mean ± SD is presented from *n* = 3 biological replicates; P was calculated by unpaired *t* test. (F) Blots show Cen protein in 1-3-h embryos and quantified in F'. Each dot is a measurement from an independent experiment; mean ± SD are displayed (red). Data in A-D' and F' are normalized to the mean relative expression of the controls from *n* = 3 biological replicates. *, *P* < 0.05; **** *P* < 0.0001 by unpaired *t* test. Full-sized blots available on FigShare (see Materials and methods). n.s., not significant.

to normal centrosome functions through in-depth studies with a model transcript, *cen* mRNA. We identified FMRP as an RNA-binding protein required for regulation of *cen* RNA localization, organization, and translational control. Further, reducing *cen* dosage rescued *Fmr1*-dependent mitotic errors and embryonic lethality. We also directly tested the consequences of mis-targeting *cen* mRNA. Mislocalization of *cen* mRNA to the anterior abrogated the normal localization of Cen to more distal centrosomes and disrupted spindle organization. Anterior mitotic divisions were also severely disrupted due to the increased local concentration of *cen* mRNA, which also recruited FMRP. These studies suggest that a normalized local concentration of *cen* mRNA is essential for normal cell division and genome stability.

Centrosomes as platforms for translational regulation

FMRP is a multifunctional RNA-binding protein with roles in translational repression, activation, RNA localization, and RNA stability (Darnell, 2011; Estes et al., 2008; Greenblatt and Spradling, 2018; Pilaz et al., 2016). In humans, mutations in the gene encoding FMRP, *FMRI*, are the leading cause of heritable intellectual disability and autism. Although high-throughput studies have identified putative RNA substrates, surprisingly few of these have been validated (Santoro et al., 2012). Our studies demonstrate that *cen* mRNA is regulated by FMRP, either directly or indirectly, and that titrating *cen* dosage is sufficient to partially restore embryonic viability in *Fmr1* mutants. Consistent with direct regulation of *cen* mRNA by

FMRP, the *cen* coding sequence contains six putative binding motifs for FMRP, according to RBPmap, an RNA-binding motif predictor (Paz et al., 2014). Moreover, human orthologues of *cen*, *CDR2* and *CDR2L*, were identified as direct FMRP targets (Ascano et al., 2012). Deregulation of *CDR2* and *CDR2L* is associated with paraneoplastic cerebellar degeneration (Albert et al., 1998; Corradi et al., 1997). Our studies suggest that *Drosophila cen* may serve as a valuable model to uncover mechanisms underlying FMRP-mediated regulation of *CDR2* and *CDR2L*. Whether FMRP similarly regulates other centrosome-localized mRNAs is an interesting question for future study.

The enhanced recruitment of *cen* mRNA to heterogeneously sized pericentrosomal granules, coupled with the increased production of Cen protein within *Fmr1* mutants, led us to speculate that *cen* mRNA granules may be sites of local translation, as recently proposed (Bergalet et al., 2020). However, disruption of *cen* granule formation, as in *cnr^{B4}* mutants, does not impair total Cen protein levels. This finding raises the possibility that Cen may be translated at alternate sites or that maternal stores of Cen obscure changes resulting from *cen* mRNA granule loss. These models are not mutually exclusive, and *cen* mRNA may be translated at multiple locales. Our data support a model in which centrosomes serve as platforms for translation control, which may be positive or negative depending on the specific transcript and/or cell cycle stage, consistent with the idea that *cen* mRNA granules are sites of Cen translational regulation (Bergalet et al., 2020).

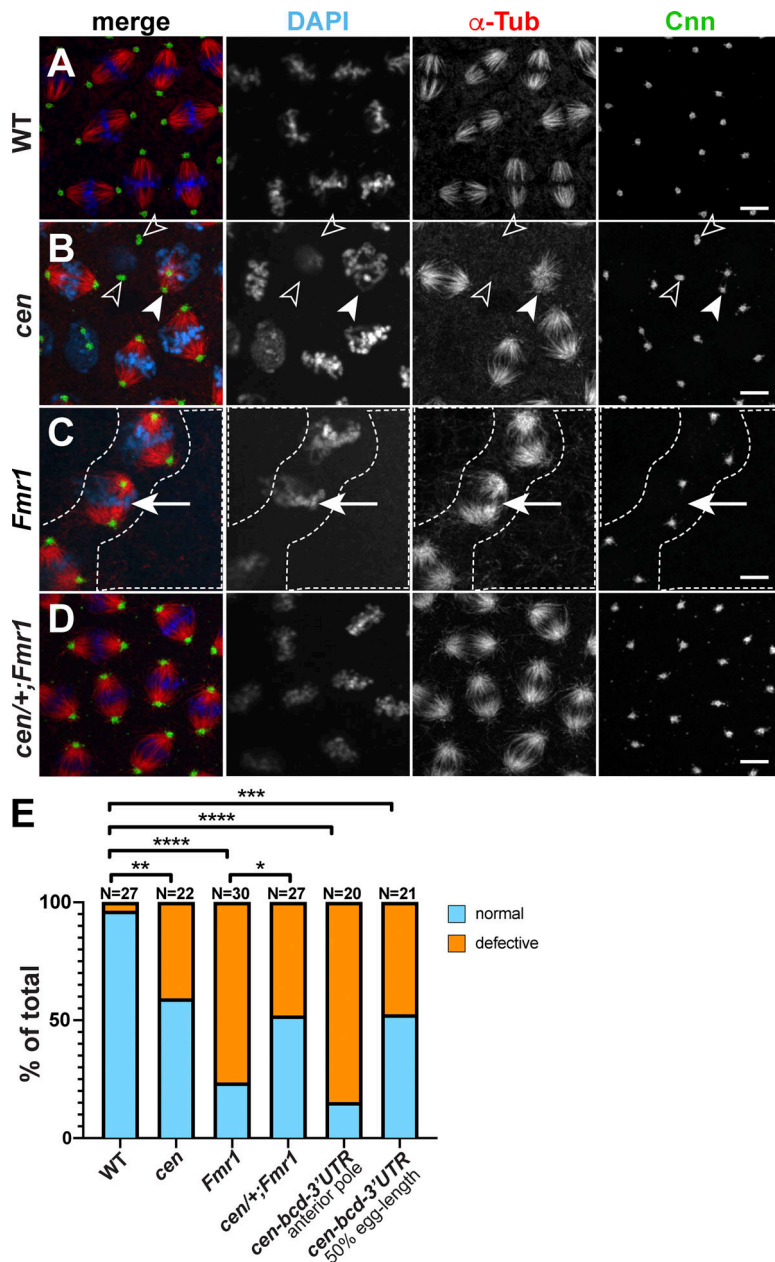


Figure 7. Cen and FMRP ensure proper mitosis. Maximum-intensity projections of metaphase NC 11 embryos from the indicated genotypes stained for β -Tub to label microtubules (red), Cnn (green), and DAPI (blue). **(A)** WT show uniform bipolar mitotic spindles. **(B)** *cen* embryo with reduced microtubules (open arrowheads) and incomplete centrosome separation (closed arrowheads). **(C)** *Fmr1* embryo with nuclear fallout (dashed lines) and bent spindles (arrows). **(D)** Hemizyosity for *cen* partially rescues *Fmr1* mutants. **(E)** Frequency of spindle defects from $n = 27$ WT, 22 *cen*, 30 *Fmr1*, 27 *cen/+;Fmr1*, 20 *cen-bcd-3'UTR* (anterior), and 21 *cen-bcd-3'UTR* (50% egg length) embryos. *, $P < 0.05$; **, $P < 0.01$; ***, $P < 0.001$; ****, $P < 0.0001$ by Fisher's exact test. Scale bars: 5 μ m.

We show that *cen* mRNA preferentially localizes to interphase centrosomes; that the centrosome scaffold, Cnn, is required for *cen* mRNA granule formation and localization; and that FMRP functions as a negative regulator of *cen* mRNA, limiting *cen* mRNA stability and translation of Cen protein (Fig. 9 E). We speculate that FMRP represses Cen translation within *cen* mRNA granules, dampening the local Cen concentration. Consequently, *cen* mRNA enrichment at centrosomes is exaggerated in *Fmr1* mutants. Other factors likely promote Cen translation. Translational repression or derepression may be coupled to *cen* mRNA granule centrosome proximity, which decreases as embryos enter mitosis. An imbalance of Cen levels at centrosomes, either too little (as in *cen* mutants) or too much (as in *Fmr1* mutants or *cen-bcd-3'UTR* embryos), impairs centrosome function/spindle integrity and embryonic viability. As the *cen* 3'UTR recruits *ik2* mRNA to centrosomes, the mitotic defects observed following

cen perturbation may result from indirect effects via *ik2* mRNA (Bergalet et al., 2020). Nonetheless, *cen* mRNA dosage must be properly regulated for mitotic fidelity.

Differential enrichment of mRNAs on interphase centrosomes

A common trend emerging from our comparative analyses is the greater enrichment of mRNA at interphase versus metaphase centrosomes. One possible explanation is the differential size of interphase centrosomes, which are significantly larger in *Drosophila* embryos owing to the elaboration of extended centrosome flares, part of the architecture of the centrosome scaffold (Lerit et al., 2015; Megraw et al., 2002; Richens et al., 2015). This pattern contrasts with mammalian centrosomes, which are larger in mitosis (Lawo et al., 2012). According to this size model, a larger centrosome might dock additional RNAs simply because of the increased volume it occupies in the cell. We discount this

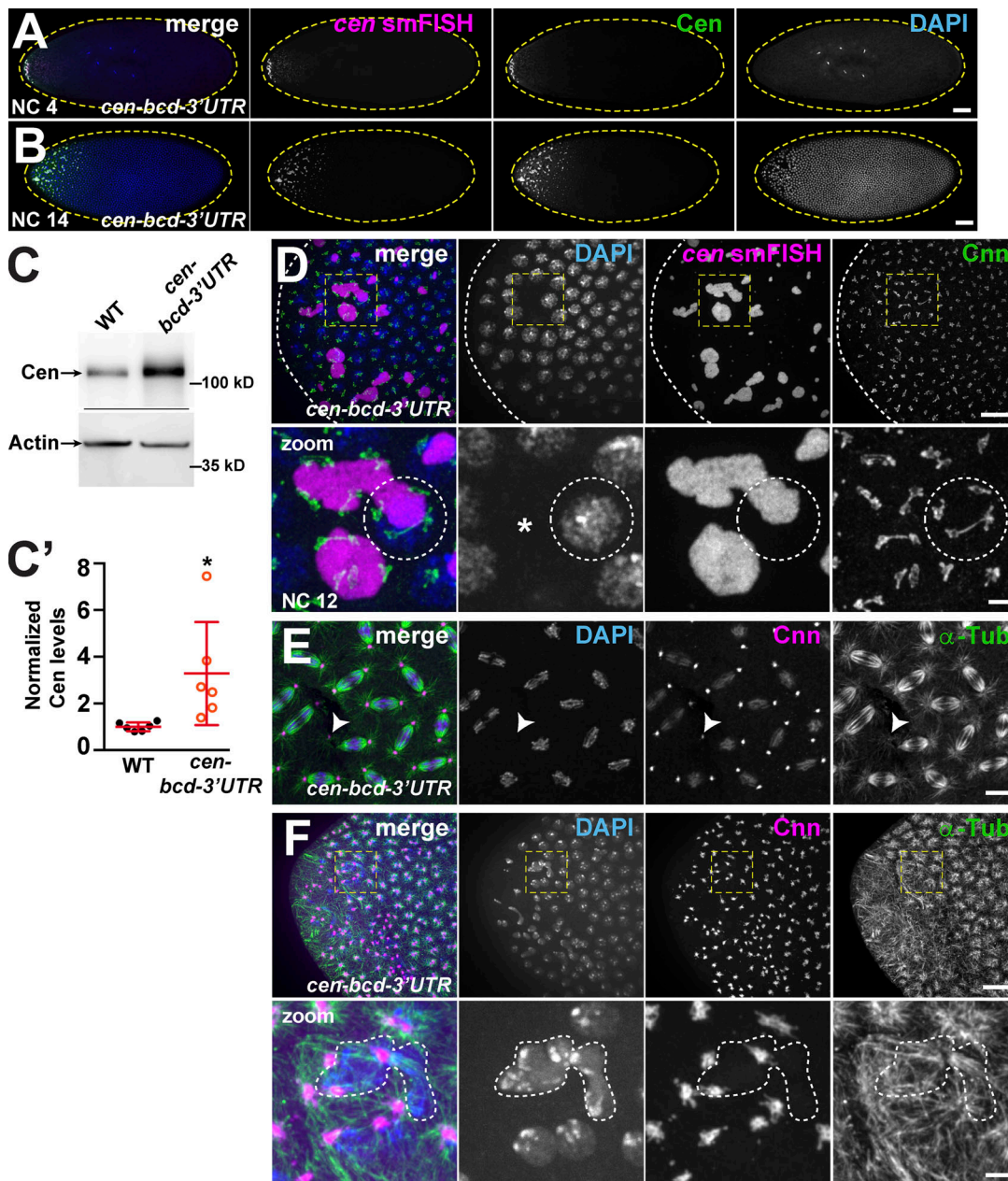


Figure 8. Ectopic localization of *cen* mRNA disrupts nuclear divisions. Maximum-intensity projections of *cen-bcd-3'UTR* embryos (derived from females expressing a *pUAS⁺cen-bcd-3'UTR* transgene and the maternal α -Tub *GAL4* driver in the *cen* null background). **(A and B)** Embryos labeled with *cen* smFISH (magenta), DAPI (blue), and Cen (green) with a gradient of *cen* mRNA and protein (A) and disrupted nuclear spacing at the anterior pole (B). **(C)** Blots show Cen protein in 1–3-h (~NC 7–NC 14) embryos and quantified in C'. Cen levels were normalized to the mean WT levels of actin from *n* = 3 independent biological replicates with *n* = 2 technical replicates run on the same gel. Mean \pm SD is displayed (red). *, *P* < 0.05 by unpaired *t* test. **(D)** NC 12 anterior with large *cen* RNPs (magenta) decorated by centrosomes (Cnn, green). Dashed circle outlines nucleus and part of a *cen* RNP with supernumerary centrosomes. **(E)** NC 12 embryo at ~50% egg length; arrowhead marks a detached centrosome. **(F)** NC 12 embryo at anterior pole with disorganized microtubules (α -Tub, green), centrosome position (Cnn, magenta), and dysmorphic nuclei (DAPI; dashed lines). Boxes enlarged below (zoom). Scale bars: 50 μ m (A and B); 10 μ m (D–F); and 2 μ m (insets).

model based on our finding that a highly expressed control transcript, *gapdh*, does not enrich at interphase centrosomes. This result also argues against the idea that centrosomes recruit RNA molecules spuriously. Relatively few RNAs localize to centrosomes (Lécuyer et al., 2007; Raff et al., 1990). We show that the localization of centrosome-associated RNA is regulated in space and time.

Why do RNAs localize to interphase centrosomes? Recent work in mammalian cells proposed that some lengthy transcripts may be cotranslationally transported to centrosomes (Chouaib et al., 2020; Sepulveda et al., 2018). This model would account for contemporaneous recruitment and colocalization of centrosome mRNA and proteins and may be pertinent to *cen* mRNA localization. Of the RNAs overlapping with the

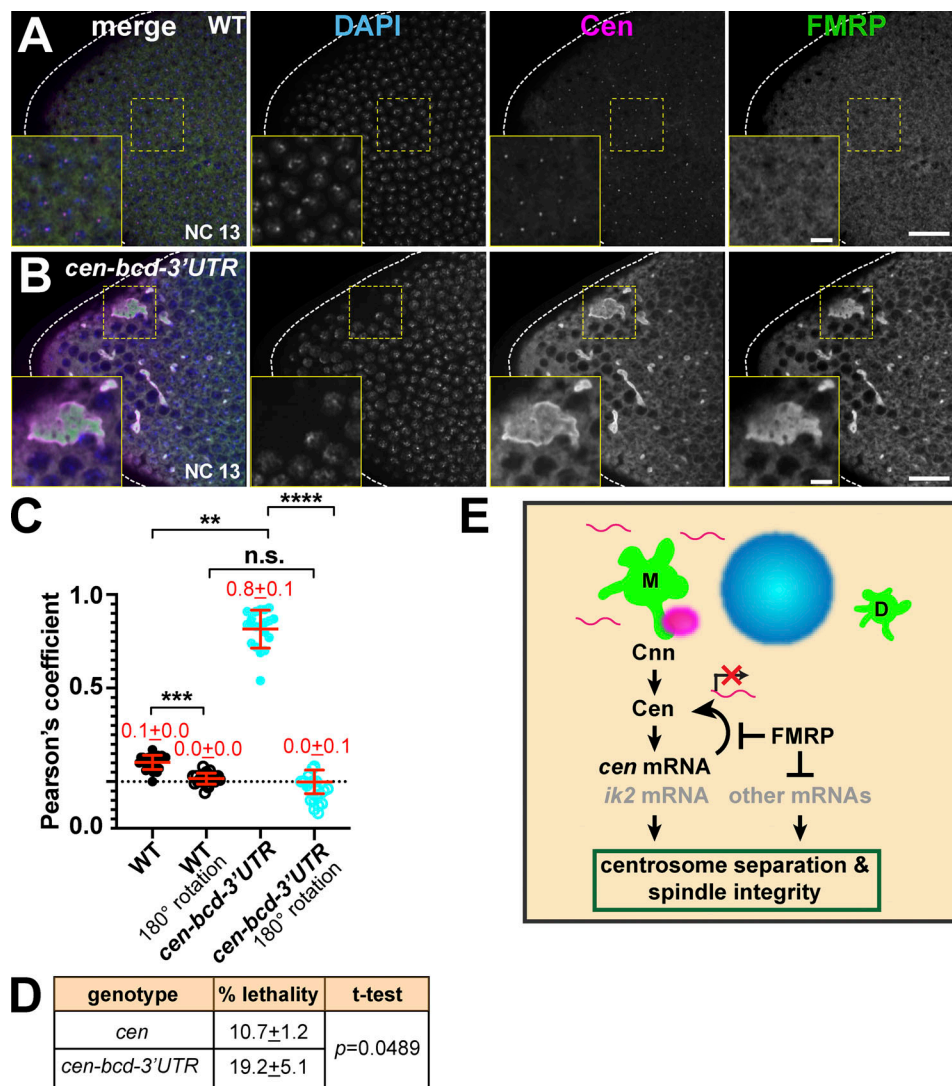


Figure 9. Deregulation of *cen* mRNA impairs viability. (A and B) Single optical sections of interphase NC 13 embryos stained for Cen and FMRP; boxes enlarged in inset. (C) Pearson's coefficient of Cen and FMRP signals; each dot is a measurement from $n = 25$ WT and $n = 19$ *cen-bcd-3'UTR* embryos from two independent experiments. One channel was rotated 180° to test for specificity of colocalization. Mean \pm SD is displayed (red). **, $P < 0.01$; ***, $P < 0.001$; ****, $P < 0.0001$ by Kruskal-Wallis followed by Dunn's multiple comparisons test. Scale bars: 20 μ m (A and B); 5 μ m (insets). n.s., not significant. (D) Embryonic lethality rates in *cen* versus *cen-bcd-3'UTR* embryos from three independent experiments. Mean \pm SD is shown; P calculated by unpaired t test. (E) Model for FMRP-mediated regulation of *cen* mRNA. A direct interaction docks Cen to Cnn (green) at the centrosome (Kao and Megraw, 2009). Cen protein interacts with *cen* mRNA (magenta), which also recruits *ik2* mRNA (Bergalet et al., 2020). Our data suggest that *cen* mRNA localization, organization into granules and levels, and translation are regulated by FMRP. Further, *cen* mRNA is an important target of FMRP required for spindle integrity and viability.

centrosome surface, *sov* was unique in that it appeared to preferentially dock along centrosome flares, localizing to the outer PCM zone. However, we do not detect *Sov* protein at centrosomes. Instead, *Sov* resides in the nucleus during interphase and is undetectable after nuclear envelope breakdown (Benner et al., 2019). These findings suggest that *Sov* is rapidly translocated into the nucleus. Live imaging of RNA transport and nascent protein synthesis is required to rigorously test the dynamics of RNA localization and local translation.

Another model that may account for enrichment of centrosome RNAs at interphase centrosomes is the possibility that RNA contributes to centrosome structure, perhaps by promoting phase transitions (Woodruff et al., 2015, 2017;

Zwicker et al., 2014). A common principle of phase transitions is the association of intrinsically disordered proteins with specific RNA molecules to form non-membrane-bound organelles with unique biophysical properties (Berry et al., 2018). Might *cen* mRNA granules represent phase-separated domains? Congruous with phase separation, Cen protein contains multiple predicted intrinsically disordered domains (Ishida and Kinoshita, 2007). While we cannot rule out the contribution of all centrosomal RNAs, our studies do not suggest that *cen* mRNA contributes to centrosome structure. Mistargeting *cen* mRNA to the anterior cortex did not appear to disrupt the organization of distal centrosomes, for example.

Critically, disrupting the PCM scaffold is sufficient to inhibit formation of the *cen* mRNA granule. We previously showed that the PCM scaffold becomes progressively more structured during the prolonged interphases of later NCs (Lerit et al., 2015). Additionally, the mother centrosome organizes a larger PCM scaffold owing to inherently greater levels of Cnn and PLP (Conduit et al., 2010; Lerit et al., 2015). Collectively, these features may account for the asymmetric localization of *cen* mRNA to mother centrosomes in late-stage syncytial embryos. These data lead us to conclude that the PCM scaffold organized by Cnn and PLP is upstream of the recruitment and organization of *cen* mRNA granules (Fig. 9 E).

Many types of RNP granules form within cells, including stress granules, germ granules, P-bodies, etc., which all have unique functions and modes of assembly. The spatial proximity of multiple RNA molecules may facilitate intermolecular RNA interactions subsequently recognized by RNA-binding proteins (Van Treeck and Parker, 2018). The FMRP-containing *cen* mRNA granule represents one such RNP, and further understanding how it promotes mitotic integrity warrants further investigation. As the early *Drosophila* embryo is transcriptionally quiescent, posttranscriptional regulatory mechanisms, and especially translational control, are fundamentally important for proper centrosome regulation and function.

Materials and methods

Fly stocks

The following *Drosophila* strains and transgenic lines were used: γ^1w^{III8} (1495; Bloomington *Drosophila* Stock Center) was used as the WT control unless otherwise noted; $P_{BAC}\text{-GFP-Cnn}$, which expresses Cnn tagged at the N-terminus with EGFP under endogenous regulatory elements (Lerit et al., 2015); $Ubi\text{-GFP-}\gamma\text{-Tub23C}$, which expresses GFP- $\gamma\text{-Tub}$ under the *Ubiquitin* promoter (Lerit and Rusan, 2013); null *cen* mutant embryos derived from homozygous *cen*^{fo4787} animals (18805; Bloomington *Drosophila* Stock Center; Kao and Megraw, 2009); null *Fmr1* mutant embryos derived from *Fmr1* ^{Δ 113M}/*Fmr1*³ trans-heterozygotes (*Fmr1* ^{Δ 113M}; 67403; Bloomington *Drosophila* Stock Center; Zhang et al., 2001); *Fmr1*³, gift from T. Jongens, University of Pennsylvania, Philadelphia, PA; Dockendorff et al., 2002); and hypomorphic *cnn*^{B4} mutants, a gift from T. Megraw (Florida State University, Tallahassee, FL). The maternal $\gamma\text{-Tub}$ promoter was used to control *GAL4* expression (*matGAL4*; 7063; Bloomington *Drosophila* Stock Center) to drive expression of *pUASp-cen-bcd-3'UTR* (this study). *FMRP-GFP* is a recombiner line expressing FMRP tagged at the C-terminus with GFP under endogenous regulatory elements (gift from M. Ramaswami, Trinity College Dublin, Dublin, Ireland; Sudhakaran et al., 2014). In all experiments, mutant embryos represent progeny derived from mutant mothers to examine maternal effects. Flies were raised on molasses-based *Drosophila* medium, and crosses were maintained at 25°C in a light- and temperature-controlled chamber.

Construction of transgenic animals

To generate *pUASp-cen-bcd-3'UTR*, the *cen* coding sequence was PCR amplified using Phusion high-fidelity DNA polymerase

from the cDNA clone LD41224 (*Drosophila* Genomics Resource Center) using the primers 5'-GCAGGCTCCGCGGCCGCCCTTC ACCAGGATGGAGGAATCCAATCACGGTTC-3' and 5'-GAAACT CTCTAACAGCCTCTCATCCAGGTTACTTTTGACGAAACTGATG ATGATGACTC-3'. The *cen* start and stop codons are underlined. The *bcd-3'UTR* was PCR amplified using Q5 high-fidelity polymerase (M0491S; New England Biolabs) from genomic DNA using the primers 5'-GAGTCATCATCATCAGTTTCGTCAAAA GTAACCTGGATGAGAGGCGTGTAGAG-3' and 5'-CTGGGT CGGCGCGCCCACCCTTGTCTAGGTAGTTAGTCACAATTTACC CGAGTAGAGTAG-3'. The *cen-bcd-3'UTR* fusion was assembled and directionally cloned into the pENTR-D vector (Invitrogen) by Gibson assembly using fivefold molar excess of the *bcd-3'UTR*. Sequence-verified single-colony clones were shuttled into the destination vector pPW (UASp promoter) using the Gateway cloning system (Invitrogen). Transgenic animals were generated by BestGene (Chino Hills, CA).

Embryonic hatch rate analysis

24-h collections of eggs were collected on yeasted grape juice agar plates, transferred to fresh plates, and aged for 48 h at 25°C. Unhatched embryos were counted from a total of ~600 embryos, and data presented are mean \pm SD from three biological replicates.

Immunofluorescence

Embryos were prepared for immunofluorescence as described in Lerit et al. (2015). Briefly, samples were fixed in PFA, blocked extensively in BBT (PBS supplemented with 0.1% Tween-20 and 0.1% BSA), and incubated overnight at 4°C with primary antibodies diluted in BBT. The next day, samples were further blocked in BBT supplemented with 2% normal goat serum and incubated with secondary antibodies and DAPI for 2 h at room temperature before being mounted in AquaPoly/Mount mounting medium (87001-902; VWR).

The following primary antibodies were used: rabbit anti-Cen (1:500; gift from T. Megraw; Kao and Megraw, 2009), rabbit anti-Cnn (1:3,500; gift from T. Megraw), mouse anti- $\alpha\text{-Tub DM1}\alpha$ (1:500; T6199; Sigma-Aldrich), rabbit anti-Egl (1:2,000; gift from R. Lehmann, New York University, New York, NY), rabbit anti-Pum (1:1,000; gift from Martine Simonelig, Institute of Human Genetics, University of Montpellier, Montpellier, France), mouse anti-Orb2 (1:1,000; clone 4G8; Developmental Studies Hybridoma Bank), mouse anti-me31B (1:3,000; gift from A. Nakamura, Kumamoto University, Kumamoto, Japan); and mouse anti-FMRP (1:10; clone 5A11; Developmental Studies Hybridoma Bank). Secondary antibodies and stains were Alexa Fluor 488, 568, or 647 (1:500, Molecular Probes). DAPI was used at 10 ng/ml (Thermo Fisher Scientific).

Detection of RNA by smFISH

smFISH experiments were adapted from manufacturer's recommended protocols. All steps were performed with RNase-free solutions. Briefly, fixed and rehydrated embryos were washed in PBST (PBS plus 0.1% Tween-20) and washed in wash buffer (WB; 10% formamide and 2 \times SSC supplemented fresh each experiment with 0.1% Tween-20 and 2 μ g/ml nuclease-free BSA

[0332-25G; VWR]). Embryos were then incubated with 100 μ l of hybridization buffer (HB; 100 mg/ml dextran sulfate and 10% formamide in 2 \times SSC supplemented fresh each experiment with 0.1% Tween-20, 2 μ g/ml nuclease-free BSA, and 10 mM ribonucleoside vanadyl complex (RVC; S1402S; New England Biolabs) for 10–20 min in a 37°C water bath. Stellaris smFISH probes conjugated to Quasar 570 dye (LGC Biosearch Technologies) were designed against the coding region for each gene of interest using the Stellaris RNA FISH probe designer and stored at –20°C as stock solutions of 25 μ M in nuclease-free water. Probes are listed in Table S1. After preincubation in HB, embryos were incubated in a 37°C water bath overnight in 25 μ l of HB containing a 1:50 dilution of smFISH probe. The next morning, embryos were washed three times for 30 min each in pre-warmed WB, stained with DAPI for 1 h at room temperature, washed with PBST, and mounted with Vectashield mounting medium (H-1000; Vector Laboratories). Slides were stored at 4°C and imaged within 1 wk.

For experiments in which immunofluorescence was combined with smFISH, we adapted a protocol from Xu et al. (2015). After overnight incubation with smFISH probes, embryos were washed well in WB, followed by two 10-min washes in 2 \times SSC–0.1% Tween-20 and four 10-min washes in PBST. Embryos were blocked for 2 h in blocking solution (PBS supplemented with 1 mg/ml nuclease-free BSA, 0.1% Tween-20, and 2 mM RVC, prepared fresh) and incubated overnight in primary antibodies at 4°C. The next day, embryos were washed well in blocking solution, incubated with secondary antibodies and DAPI at room temperature, and washed in PBST before being mounted in Vectashield.

Microscopy

Images were acquired on a Nikon Ti-E system fitted with a Yokogawa CSU-X1 spinning disk head (Yokogawa Corp. of America), Orca Flash 4.0 v2 digital complementary metal-oxide-semiconductor camera (Hamamatsu Corp.), Perfect Focus system (Nikon), and a Nikon LU-N4 solid-state laser launch (15 mW; 405, 488, 561, and 647 nm) using the following Nikon objectives: 100 \times 1.49-NA Apo total internal reflection fluorescence oil immersion, 40 \times 1.3-NA Plan Fluor oil immersion, and 20 \times 0.75-NA Plan Apo. Images were acquired at ambient temperature (~25°C) using either Vectashield or Aqua-Poly/Mount imaging medium, as described. The microscope was powered through Nikon Elements AR software on a 64-bit HP Z440 workstation (Hewlett-Packard).

Image analysis

For fixed studies, Alexa Fluor 488, 568, or 647 was used. Images were assembled using Fiji (National Institutes of Health; Schindelin et al., 2012), Adobe Photoshop, and Adobe Illustrator software to separate or merge channels, crop regions of interest, generate maximum-intensity projections, and adjust brightness and contrast.

RNA detection and measurements

For quantification of single-molecule RNA distribution relative to centrosomes, single-channel .tif raw images were segmented

in three dimensions using code adapted from the Allen Institute for Cell Science Cell Segmenter (Chen et al., 2018). Each segmented image was compared with the original image to validate accurate segmentation. RNA objects of ≥ 50 pixels in segmented images were identified, and object features were extracted. Extracted features included the raw image total pixel intensity, the object centroid coordinates, and the surface coordinates. Distances were measured from the surface of each RNA object to the surface of the closest centrosome.

For single-molecule normalization, we used a previously described method (Mueller et al., 2013). Single molecules of RNA are objects of 50–100 pixels, as determined by their diffraction-limited 200-nm size. For each RNA probe, we divided the integrated intensity of each RNA object by the averaged integrated intensity of all single-molecule RNAs, allowing an estimate of the number of RNA molecules per object. We then calculated the percentage of total RNA that overlapped with centrosomes. For *cen* and *gapdh* mRNAs, we calculated the percentage of RNA in granules, which is the fraction of RNA contained in objects estimated to have ≥ 4 RNAs. We selected 10 and 4 μ m as the upper boundary for the pseudocell radius for NC 10 and NC 13, respectively, based on measuring the centrosome-to-centrosome distances from a set of representative images. A detailed protocol for RNA analysis was recently described (Ryder and Lerit, 2020).

Spindle morphology defects

Mitotic embryos imaged at 40 \times were examined for the following morphologies: bent spindles, multipolar or fused spindles, acentrosomal spindle poles, and defective centrosome separation. If any spindles within an embryo contained one of these phenotypes, the embryo was considered positive for a spindle morphology defect. Three independent biological replicates were performed for each genotype.

Colocalization analysis

Single optical slices were selected for analysis. For analysis of Cen protein overlap with *cen* RNA, the entire image was analyzed. For analysis of FMRP overlap with Cen protein in *cen-bcd-3'UTR* embryos, a 40 \times 40- μ m region of interest was selected using the Cen protein channel to include Cen protein aggregates. Colocalization was measured on background-subtracted and automatic threshold-masked images using the Coloc 2 plugin for Fiji (Schindelin et al., 2012).

Immunoblotting

Aged embryos were harvested, dechorionated in bleach, flash frozen in liquid nitrogen, and stored at –80°C. 5–10 mg of frozen embryos were lysed with a 1-ml glass dounce homogenizer (Wheaton) in 100 μ l lysis buffer (50 mM Hepes, 150 mM NaCl, 2.5 mM MgCl₂, 0.1% Triton X-100, and 250 mM sucrose supplemented with 1 \times EDTA-free protease inhibitor cocktail [04693159001; Roche], 1 μ g/ml Pepstatin A (P5318; Sigma-Aldrich), 1 mM DTT (1019777001; Sigma-Aldrich), and 2 mM RVC). 25 μ l of 5 \times SDS loading dye was added and samples were boiled for 10 min at 95°C then resolved by SDS-PAGE gel and transferred to nitrocellulose membrane by wet transfer.

Membranes were blocked for 1 h at room temperature in a 5% dry milk solution diluted in TBST (Tris-based saline with 0.05% Tween-20), washed well with TBST, and incubated overnight at 4°C with primary antibodies. After washing with TBST, membranes were incubated for 1 h in the following secondary antibodies diluted 1:5,000 in TBST, 5% milk: goat anti-mouse HRP (31430; Thermo Fisher Scientific) and goat anti-rabbit HRP (31460, Thermo Fisher Scientific). Membranes were washed well in TBST, and bands were visualized with Clarity ECL substrate (1705061; Bio-Rad) on a Bio-Rad ChemiDoc imaging system.

Densitometry was measured using Fiji software using the region-of-interest measure tool. For each sample, the ratio between the protein of interest and a loading control (e.g., β -Tub) was calculated. The mean relative expression and SD were calculated and normalized to the mean of the biological control. Three independent biological replicates were processed on the same gel.

The following primary antibodies were used: rabbit anti-Cen (1:1,000; gift from T. Megraw), mouse anti-FMRP (1:100; clone 5A11; Developmental Studies Hybridoma Bank); mouse anti- β -Tub (1:1,000; E7; Developmental Studies Hybridoma Bank); and mouse anti-actin (1:1,000; clone JLA20; Developmental Studies Hybridoma Bank).

Immunoprecipitation

~30 mg of frozen embryos were lysed with a glass dounce in 100 μ l lysis buffer (50 mM Hepes, pH 7.4, 150 mM NaCl, 2.5 mM MgCl₂, 250 mM sucrose, and 0.1% Triton X-100) supplemented with 1 \times protease inhibitor cocktail, 1 μ g/ml Pepstatin A, 1 mM DTT, 1 U/ μ l RNase Inhibitor (M0314S; New England Biolabs), and 2 mM RVC. Lysates were cleared by centrifugation, and the supernatant was precleared in 25 μ l of washed Protein A/G magnetic agarose beads (88802; Pierce), or blocked magnetic beads (bmp-20; Chromotek) for GFP-Trap of FMRP-GFP, to reduce nonspecific binding. A 0.1 volume of precleared lysates was reserved as input, and the remainder was immunoprecipitated for 2 h at 4°C in rabbit anti-GFP (A-11122; Invitrogen), rabbit anti-Cen, or no antibody as a control and transferred to 25 μ l washed Protein A/G magnetic agarose beads for immunoprecipitation for 2 h. GFP-Trap magnetic agarose beads (gtma-10; Chromotek) were used for FMRP-GFP. Beads were then washed well in immunoprecipitation buffer (lysis buffer with 8 U/ml RNase Out and 0.4 mM RVC) and resuspended in 100 μ l immunoprecipitation buffer. 50 μ l of the beads (20% of volume for GFP-Trap) were analyzed for protein content by SDS-PAGE as described above. RNA was extracted from the other 50 μ l of beads (80% of volume for GFP-Trap) using TRI Reagent (T9424; Sigma-Aldrich) and treated with TURBO DNase (AM2238; Thermo Fisher Scientific) before RT-PCR.

cDNA was synthesized from 500 ng of RNA using Superscript IV Reverse Transcriptase (18091050; Thermo Fisher Scientific) according to the manufacturer's protocol with (RT+) or without (RT-) reverse transcriptase. DNA was amplified by PCR using Phusion High Fidelity DNA Polymerase (M0530L; New England Biolabs). The following primers were used: *cen* forward, 5'-TAA CCGCAGACGGACAAC-3', and reverse, 5'-GAATGCCCTATGGCT AGAAT-3'; *gapdh* forward, 5'-CACCCATTCGTCTGTTCG-3', and reverse, 5'-CAACAGTGATTCCCGACCAG-3'; *Fmr1* forward,

5'-CATCGTTTCGACGGAGTAACA-3', and reverse, 5'-GGAGCT TGTTGTTGGCTGAT-3'; and *His3.3B* forward, 5'-CACTCCAAC AACTGTCCAGC-3', and reverse, 5'-GTCCAGCCGACGTTAGAT TG-3'.

qPCR

RNA was extracted from ~5 mg of frozen embryos using TRI Reagent and treated with Ambion Turbo DNase (AM2238; Thermo Fisher Scientific) for 30 min at 37°C, followed by phenol:chloroform extraction. On the same day, RNA concentrations were measured with a spectrophotometer, and cDNA was synthesized from 500 ng of RNA using the iScript kit according to the manufacturer's protocol (170-8891; Bio-Rad).

qPCR was performed on a Bio-Rad CFX96 real-time system with iTaq Universal SYBR Green Supermix (172-5121; Bio-Rad). Three biological samples were tested in triplicate using 96-well plates (HSP9601; Bio-Rad). *cen* expression levels were normalized to Ribosomal protein L32 (*RP49*). The following primers were used: *cen* forward, 5'-TGAGGATACGACGCTCTGTG-3', and reverse, 5'-AAAGTACCCCGGTAACACC-3', amplicon 78 bp; and *RP49* forward, 5'-CATACAGGCCCAAGATCGTG-3', and reverse, 5'-ACAGCTTAGCATATCGATCCG-3', amplicon 75 bp.

Statistical analysis

Data were plotted and statistical analysis was performed using Microsoft Excel and GraphPad Prism software. To calculate significance, the distribution was first tested for outliers using the ROUT test with $Q = 1\%$. Identified outliers were excluded from further analysis. Normality was then assessed with a D'Agnostino and Pearson normality test. Data were analyzed by Student's two-tailed *t* test, ANOVA, Fisher's exact test, or the appropriate nonparametric tests and are displayed as mean \pm SD. Data for the percentage of RNA overlapping with centrosomes presented in Figs. 1 and 2 were analyzed as one dataset for each developmental stage using the appropriate one-way ANOVA test. Data shown are representative results from at least two independent experiments, as indicated in the figure legends.

Data availability

All code for RNA detection and measurements are available on github at <https://github.com/pearlryder/rna-at-centrosomes> and <https://github.com/pearlryder/cen-at-fmr-null-centrosomes>. Full-sized images of all DNA gels and immunoblots are available at FigShare: doi.org/10.6084/m9.figshare.12821564 and doi.org/10.6084/m9.figshare.12821579.

Online supplemental material

Fig. S1 shows the workflow used to analyze mRNA localization. Fig. S2 shows that the centrosome scaffold is required for *cen* mRNA granule formation. Fig. S3 shows that *cen* mRNA granules form precociously in *cen-bcd-3'UTR* embryos. Table S1 lists all smFISH probes used in this study.

Acknowledgments

We thank Drs. Liz Gavis, Nasser Rusan, Tim Megraw, Greg Rogers, Ruth Lehmann, Mani Ramaswami, Martine Simonelig,

Akira Nakamura, and Tom Jongens for gifts of reagents; Lauren Lym and Jina Lee for technical assistance; and L. Gavis, N. Rusan, and members of our laboratory for constructive feedback.

Stocks obtained from the Bloomington *Drosophila* Stock Center (National Institutes of Health grant P40OD018537); antibodies from the Developmental Studies Hybridoma Bank, created by the National Institute of Child Health and Human Development of the National Institutes of Health and maintained at the University of Iowa Department of Biology; and reagents from the *Drosophila* Genomics Resource Center (National Institutes of Health grant 2P40OD010949) were used in this study. This work was supported by National Institutes of Health grants 5K12GM000680 and 1F32GM128407 to P.V. Ryder, National Institutes of Health grants 5K22HL126922 and 1R01GM138544 to D.A. Lerit, and American Heart Association grant 20POST35210023 to J. Fang.

The authors declare no competing financial interests.

Author contributions: P.V. Ryder and D.A. Lerit conceived of the project and designed experiments to visualize and measure centrosome RNA localization. P.V. Ryder performed and analyzed all smFISH, qPCR, immunofluorescence, and Cen blotting experiments and collaborated with J. Fang for *Fmr1* mutant data. J. Fang designed and performed FMRP biochemistry. D.A. Lerit analyzed centrosome asymmetry data, generated the *cen-bcd-3'UTR* transgenic animal, and supervised the project. All authors contributed to manuscript preparation.

Submitted: 14 April 2020

Revised: 12 September 2020

Accepted: 14 October 2020

References

- Albert, M.L., J.C. Darnell, A. Bender, L.M. Francisco, N. Bhardwaj, and R.B. Darnell. 1998. Tumor-specific killer cells in paraneoplastic cerebellar degeneration. *Nat. Med.* 4:1321–1324. <https://doi.org/10.1038/3315>
- Alliego, M.C., and M.A. Alliego. 2008. Centrosomal RNA correlates with intron-poor nuclear genes in *Spisula* oocytes. *Proc. Natl. Acad. Sci. USA.* 105:6993–6997. <https://doi.org/10.1073/pnas.0802293105>
- Alliego, M.C., M.A. Alliego, and R.E. Palazzo. 2006. Centrosome-associated RNA in surf clam oocytes. *Proc. Natl. Acad. Sci. USA.* 103:9034–9038. <https://doi.org/10.1073/pnas.0602859103>
- Anderson, K.V., and J.A. Lengyel. 1979. Rates of synthesis of major classes of RNA in *Drosophila* embryos. *Dev. Biol.* 70:217–231. [https://doi.org/10.1016/0012-1606\(79\)90018-6](https://doi.org/10.1016/0012-1606(79)90018-6)
- Ascano, M. Jr., N. Mukherjee, P. Bandaru, J.B. Miller, J.D. Nusbaum, D.L. Corcoran, C. Langlois, M. Munschauer, S. Dewell, M. Hafner, et al. 2012. FMRP targets distinct mRNA sequence elements to regulate protein expression. *Nature.* 492:382–386. <https://doi.org/10.1038/nature11737>
- Banerjee, A., M.F. Ifrim, A.N. Valdez, N. Raj, and G.J. Bassell. 2018. Aberrant RNA translation in fragile X syndrome: From FMRP mechanisms to emerging therapeutic strategies. *Brain Res.* 1693(Pt A):24–36. <https://doi.org/10.1016/j.brainres.2018.04.008>
- Benner, L., E.A. Castro, C. Whitworth, K.J.T. Venken, H. Yang, J. Fang, B. Oliver, K.R. Cook, and D.A. Lerit. 2019. *Drosophila* Heterochromatin Stabilization Requires the Zinc-Finger Protein Small Ovary. *Genetics.* 213:877–895. <https://doi.org/10.1534/genetics.119.302590>
- Bergalet, J., D. Patel, F. Legendre, C. Lapointe, L.P. Benoit Bouvrette, A. Chin, M. Blanchette, E. Kwon, and E. Lecuyer. 2020. Inter-dependent Centrosomal Co-localization of the cen and ik2 cis-Natural Antisense mRNAs in *Drosophila*. *Cell Rep.* 30:3339–3352.e3336.
- Berry, J., C.P. Brangwynne, and M. Haataja. 2018. Physical principles of intracellular organization via active and passive phase transitions. *Rep. Prog. Phys.* 81:046601. <https://doi.org/10.1088/1361-6633/aaa61e>
- Blower, M.D., E. Feric, K. Weis, and R. Heald. 2007. Genome-wide analysis demonstrates conserved localization of messenger RNAs to mitotic microtubules. *J. Cell Biol.* 179:1365–1373. <https://doi.org/10.1083/jcb.200705163>
- Chen, J., L. Ding, M.P. Viana, M.C. Hendershott, R. Yang, I.A. Mueller, and S.M. Rafelski. 2018. The Allen Cell Structure Segmenter: a new open source toolkit for segmenting 3D intracellular structures in fluorescence microscopy images. *bioRxiv*. Preprint posted December 8, 2018.
- Chouaib, R., A. Safieddine, X. Pichon, A. Imbert, O.S. Kwon, A. Samacoits, A.M. Traboulsi, M.C. Robert, N. Tsanov, E. Coleno, et al. 2020. A Dual Protein-mRNA Localization Screen Reveals Compartmentalized Translation and Widespread Co-translational RNA Targeting. *Dev. Cell.* 54:773–791.e5. <https://doi.org/10.1016/j.devcel.2020.07.010>
- Conduit, P.T., K. Brunk, J. Dobbelaere, C.I. Dix, E.P. Lucas, and J.W. Raff. 2010. Centrioles regulate centrosome size by controlling the rate of Cnn incorporation into the PCM. *Curr. Biol.* 20:2178–2186. <https://doi.org/10.1016/j.cub.2010.11.011>
- Conduit, P.T., Z. Feng, J.H. Richens, J. Baumbach, A. Wainman, S.D. Bakshi, J. Dobbelaere, S. Johnson, S.M. Lea, and J.W. Raff. 2014. The centrosome-specific phosphorylation of Cnn by Polo/Plk1 drives Cnn scaffold assembly and centrosome maturation. *Dev. Cell.* 28:659–669. <https://doi.org/10.1016/j.devcel.2014.02.013>
- Conduit, P.T., A. Wainman, and J.W. Raff. 2015. Centrosome function and assembly in animal cells. *Nat. Rev. Mol. Cell Biol.* 16:611–624. <https://doi.org/10.1038/nrm4062>
- Corradi, J.P., C. Yang, J.C. Darnell, J. Dalmau, and R.B. Darnell. 1997. A post-transcriptional regulatory mechanism restricts expression of the paraneoplastic cerebellar degeneration antigen cdr2 to immune privileged tissues. *J. Neurosci.* 17:1406–1415. <https://doi.org/10.1523/JNEUROSCI.17-04-01406.1997>
- Dalby, B., and D.M. Glover. 1992. 3' non-translated sequences in *Drosophila* cyclin B transcripts direct posterior pole accumulation late in oogenesis and peri-nuclear association in syncytial embryos. *Development.* 115:989–997.
- Darnell, J.C. 2011. Defects in translational regulation contributing to human cognitive and behavioral disease. *Curr. Opin. Genet. Dev.* 21:465–473. <https://doi.org/10.1016/j.gde.2011.05.002>
- Deshpande, G., G. Calhoun, and P. Schedl. 2006. The *Drosophila* fragile X protein dFMR1 is required during early embryogenesis for pole cell formation and rapid nuclear division cycles. *Genetics.* 174:1287–1298. <https://doi.org/10.1534/genetics.106.062414>
- Dienstbier, M., F. Boehl, X. Li, and S.L. Bullock. 2009. Egalitarian is a selective RNA-binding protein linking mRNA localization signals to the dynein motor. *Genes Dev.* 23:1546–1558. <https://doi.org/10.1101/gad.531009>
- Dockendorff, T.C., H.S. Su, S.M.J. McBride, Z. Yang, C.H. Choi, K.K. Siwicki, A. Sehgal, and T.A. Jongens. 2002. *Drosophila* lacking *dFmr1* activity show defects in circadian output and fail to maintain courtship interest. *Neuron.* 34:973–984. [https://doi.org/10.1016/S0896-6273\(02\)00724-9](https://doi.org/10.1016/S0896-6273(02)00724-9)
- Estes, P.S., M. O'Shea, S. Clasen, and D.C. Zarnescu. 2008. Fragile X protein controls the efficacy of mRNA transport in *Drosophila* neurons. *Mol. Cell. Neurosci.* 39:170–179. <https://doi.org/10.1016/j.mcn.2008.06.012>
- Foe, V.E., and B.M. Alberts. 1983. Studies of nuclear and cytoplasmic behaviour during the five mitotic cycles that precede gastrulation in *Drosophila* embryogenesis. *J. Cell Sci.* 61:31–70.
- Foe, V.E., G.M. Odell, and B.A. Edgar. 1993. Mitosis and morphogenesis in the *Drosophila* embryo: Point and counterpoint. *ScienceOpen.* 149–300.
- Gamberi, C., O. Johnstone, and P. Lasko. 2006. *Drosophila* RNA Binding Proteins. *Int. Rev. Cytol.* 248:43–139.
- Glover, D.M., M.H. Leibowitz, D.A. McLean, and H. Parry. 1995. Mutations in aurora prevent centrosome separation leading to the formation of monopolar spindles. *Cell.* 81:95–105. [https://doi.org/10.1016/0092-8674\(95\)90374-7](https://doi.org/10.1016/0092-8674(95)90374-7)
- Graveley, B.R., A.N. Brooks, J.W. Carlson, M.O. Duff, J.M. Landolin, L. Yang, C.G. Artieri, M.J. van Baren, N. Boley, B.W. Booth, et al. 2011. The developmental transcriptome of *Drosophila melanogaster*. *Nature.* 471:473–479. <https://doi.org/10.1038/nature09715>
- Greenblatt, E.J., and A.C. Spradling. 2018. Fragile X mental retardation 1 gene enhances the translation of large autism-related proteins. *Science.* 361:709–712. <https://doi.org/10.1126/science.aas9963>
- Ishida, T., and K. Kinoshita. 2007. PrDOS: prediction of disordered protein regions from amino acid sequence. *Nucleic Acids Res.* 35(Web Server):W460–W464. <https://doi.org/10.1093/nar/gkm363>
- Kao, L.-R., and T.L. Megraw. 2009. Centrocortin cooperates with centrosomin to organize *Drosophila* embryonic cleavage furrows. *Curr. Biol.* 19:937–942. <https://doi.org/10.1016/j.cub.2009.04.037>

- Lambert, J.D., and L.M. Nagy. 2002. Asymmetric inheritance of centrosomally localized mRNAs during embryonic cleavages. *Nature*. 420: 682–686. <https://doi.org/10.1038/nature01241>
- Lawo, S., M. Hasegan, G.D. Gupta, and L. Pelletier. 2012. Subdiffraction imaging of centrosomes reveals higher-order organizational features of pericentriolar material. *Nat. Cell Biol.* 14:1148–1158. <https://doi.org/10.1038/ncb2591>
- Lécuyer, E., H. Yoshida, N. Parthasarathy, C. Alm, T. Babak, T. Cerovina, T.R. Hughes, P. Tomancak, and H.M. Krause. 2007. Global analysis of mRNA localization reveals a prominent role in organizing cellular architecture and function. *Cell*. 131:174–187. <https://doi.org/10.1016/j.cell.2007.08.003>
- Lerit, D.A., and N.M. Rusan. 2013. PLP inhibits the activity of interphase centrosomes to ensure their proper segregation in stem cells. *J. Cell Biol.* 202:1013–1022. <https://doi.org/10.1083/jcb.201303141>
- Lerit, D.A., H.A. Jordan, J.S. Poulton, C.J. Fagerstrom, B.J. Galletta, M. Peifer, and N.M. Rusan. 2015. Interphase centrosome organization by the PLP-Cnn scaffold is required for centrosome function. *J. Cell Biol.* 210:79–97. <https://doi.org/10.1083/jcb.201503117>
- Ling, S.C., P.S. Fahrner, W.T. Greenough, and V.I. Gelfand. 2004. Transport of *Drosophila* fragile X mental retardation protein-containing ribonucleoprotein granules by kinesin-1 and cytoplasmic dynein. *Proc. Natl. Acad. Sci. USA*. 101:17428–17433. <https://doi.org/10.1073/pnas.0408114101>
- Little, S.C., K.S. Sinsimer, J.J. Lee, E.F. Wieschaus, and E.R. Gavis. 2015. Independent and coordinate trafficking of single *Drosophila* germ plasm mRNAs. *Nat. Cell Biol.* 17:558–568.
- Macdonald, P.M., and G. Struhl. 1988. cis-acting sequences responsible for anterior localization of bicoid mRNA in *Drosophila* embryos. *Nature*. 336:595–598. <https://doi.org/10.1038/336595a0>
- Magescas, J., J.C. Zonka, and J.L. Feldman. 2019. A two-step mechanism for the inactivation of microtubule organizing center function at the centrosome. *eLife*. 8:E47867. <https://doi.org/10.7554/eLife.47867>
- Marshall, W.F., and J.L. Rosenbaum. 2000. Are there nucleic acids in the centrosome? *Curr. Top. Dev. Biol.* 49:187–205. [https://doi.org/10.1016/S0070-2153\(99\)49009-X](https://doi.org/10.1016/S0070-2153(99)49009-X)
- Martinez-Campos, M., R. Basto, J. Baker, M. Kernan, and J.W. Raff. 2004. The *Drosophila* pericentrin-like protein is essential for cilia/flagella function, but appears to be dispensable for mitosis. *J. Cell Biol.* 165:673–683. <https://doi.org/10.1083/jcb.200402130>
- Megraw, T.L., S. Kilaru, F.R. Turner, and T.C. Kaufman. 2002. The centrosome is a dynamic structure that ejects PCM flares. *J. Cell Sci.* 115: 4707–4718. <https://doi.org/10.1242/jcs.00134>
- Megraw, T.L., K. Li, L.R. Kao, and T.C. Kaufman. 1999. The centrosomin protein is required for centrosome assembly and function during cleavage in *Drosophila*. *Development*. 126:2829–2839.
- Mittasch, M., V.M. Tran, M.U. Rios, A.W. Fritsch, S.J. Enos, B. Ferreira Gomes, A. Bond, M. Kreysing, and J.B. Woodruff. 2020. Regulated changes in material properties underlie centrosome disassembly during mitotic exit. *J. Cell Biol.* 219:647. <https://doi.org/10.1083/jcb.201912036>
- Monzo, K., O. Papoulas, G.T. Cantin, Y. Wang, J.R. Yates III, and J.C. Sisson. 2006. Fragile X mental retardation protein controls trailer hitch expression and cleavage furrow formation in *Drosophila* embryos. *Proc. Natl. Acad. Sci. USA*. 103:18160–18165. <https://doi.org/10.1073/pnas.0606508103>
- Mueller, F., A. Senecal, K. Tantale, H. Marie-Nelly, N. Ly, O. Collin, E. Basyuk, E. Bertrand, X. Darzacq, and C. Zimmer. 2013. FISH-quant: automatic counting of transcripts in 3D FISH images. *Nat. Methods*. 10:277–278. <https://doi.org/10.1038/nmeth.2406>
- Nigg, E.A., and J.W. Raff. 2009. Centrioles, centrosomes, and cilia in health and disease. *Cell*. 139:663–678. <https://doi.org/10.1016/j.cell.2009.10.036>
- Palazzo, R.E., J.M. Vogel, B.J. Schnackenberg, D.R. Hull, and X. Wu. 2000. Centrosome maturation. *Curr. Top. Dev. Biol.* 49:449–470. [https://doi.org/10.1016/S0070-2153\(99\)49021-0](https://doi.org/10.1016/S0070-2153(99)49021-0)
- Papoulas, O., K.F. Monzo, G.T. Cantin, C. Ruse, J.R. Yates III, Y.H. Ryu, and J.C. Sisson. 2010. dFMRP and Caprin, translational regulators of synaptic plasticity, control the cell cycle at the *Drosophila* mid-blastula transition. *Development*. 137:4201–4209. <https://doi.org/10.1242/dev.055046>
- Paz, I., I. Kostli, M. Ares Jr., M. Cline, and Y. Mandel-Gutfreund. 2014. RBPmap: a web server for mapping binding sites of RNA-binding proteins. *Nucleic Acids Res.* 42(W1):W361–W367. <https://doi.org/10.1093/nar/gku406>
- Pilaz, L.-J., A.L. Lennox, J.P. Rouanet, and D.L. Silver. 2016. Dynamic mRNA Transport and Local Translation in Radial Glial Progenitors of the Developing Brain. *Curr. Biol.* 26:3383–3392. <https://doi.org/10.1016/j.cub.2016.10.040>
- Raff, J.W., W.G. Whitfield, and D.M. Glover. 1990. Two distinct mechanisms localise cyclin B transcripts in syncytial *Drosophila* embryos. *Development*. 110:1249–1261.
- Raj, A., P. van den Bogaard, S.A. Rifkin, A. van Oudenaarden, and S. Tyagi. 2008. Imaging individual mRNA molecules using multiple singly labeled probes. *Nat. Methods*. 5:877–879. <https://doi.org/10.1038/nmeth.1253>
- Richens, J.H., T.P. Barros, E.P. Lucas, N. Peel, D.M.S. Pinto, A. Wainman, and J.W. Raff. 2015. The *Drosophila* Pericentrin-like-protein (PLP) cooperates with Cnn to maintain the integrity of the outer PCM. *Biol. Open*. 4: 1052–1061. <https://doi.org/10.1242/bio.012914>
- Ryder, P.V., and D.A. Lerit. 2020. Quantitative analysis of subcellular distributions with an open-source, object-based tool. *Biology Open*. 9. <https://doi.org/10.1242/bio.055228>
- Ryder, P.V., and D.A. Lerit. 2018. RNA localization regulates diverse and dynamic cellular processes. *Traffic*. 19:496–502. <https://doi.org/10.1111/tra.12571>
- Santoro, M.R., S.M. Bray, and S.T. Warren. 2012. Molecular mechanisms of fragile X syndrome: a twenty-year perspective. *Annu. Rev. Pathol.* 7: 219–245. <https://doi.org/10.1146/annurev-pathol-011811-132457>
- Schindelin, J., I. Arganda-Carreras, E. Frise, V. Kaynig, M. Longair, T. Pietzsch, S. Preibisch, C. Rueden, S. Saalfeld, B. Schmid, et al. 2012. Fiji: an open-source platform for biological-image analysis. *Nat. Methods*. 9: 676–682. <https://doi.org/10.1038/nmeth.2019>
- Sepulveda, G., M. Antkowiak, I. Brust-Mascher, K. Mahe, T. Ou, N.M. Castro, L.N. Christensen, L. Cheung, X. Jiang, D. Yoon, et al. 2018. Co-translational protein targeting facilitates centrosomal recruitment of PCNT during centrosome maturation in vertebrates. *eLife*. 7:e34959. <https://doi.org/10.7554/eLife.34959>
- Singh, G., G. Pratt, G.W. Yeo, and M.J. Moore. 2015. The Clothes Make the mRNA: Past and Present Trends in mRNP Fashion. *Annu. Rev. Biochem.* 84:325–354. <https://doi.org/10.1146/annurev-biochem-080111-092106>
- Sudhakaran, I.P., J. Hillebrand, A. Dervan, S. Das, E.E. Holohan, J. Hülsmeier, M. Sarov, R. Parker, K. VijayRaghavan, and M. Ramaswami. 2014. FMRP and Ataxin-2 function together in long-term olfactory habituation and neuronal translational control. *Proc. Natl. Acad. Sci. USA*. 111: E99–E108. <https://doi.org/10.1073/pnas.1309543111>
- Sullivan, W., P. Fogarty, and W. Theurkauf. 1993. Mutations affecting the cytoskeletal organization of syncytial *Drosophila* embryos. *Development*. 118:1245–1254.
- Sunkel, C.E., and D.M. Glover. 1988. polo, a mitotic mutant of *Drosophila* displaying abnormal spindle poles. *J. Cell Sci.* 89:25–38.
- Van Treeck, B., and R. Parker. 2018. Emerging Roles for Intermolecular RNA-RNA Interactions in RNP Assemblies. *Cell*. 174:791–802. <https://doi.org/10.1016/j.cell.2018.07.023>
- Vardy, L., and T.L. Orr-Weaver. 2007. The *Drosophila* PNG kinase complex regulates the translation of cyclin B. *Dev. Cell*. 12:157–166. <https://doi.org/10.1016/j.devcel.2006.10.017>
- Vastenhouw, N.L., W.X. Cao, and H.D. Lipshitz. 2019. The maternal-to-zygotic transition revisited. *Development*. 146:dev161471. <https://doi.org/10.1242/dev.161471>
- Vertii, A., H. Hehnyly, and S. Doxsey. 2016. The Centrosome, a Multitalented Renaissance Organelle. *Cold Spring Harb. Perspect. Biol.* 8:a025049. <https://doi.org/10.1101/cshperspect.a025049>
- Woodruff, J.B., B. Ferreira Gomes, P.O. Widlund, J. Mahamid, A. Honigsmann, and A.A. Hyman. 2017. The Centrosome Is a Selective Condensate that Nucleates Microtubules by Concentrating Tubulin. *Cell*. 169:1066–1077.e10. <https://doi.org/10.1016/j.cell.2017.05.028>
- Woodruff, J.B., O. Wueseke, V. Viscardi, J. Mahamid, S.D. Ochoa, J. Bunkenborg, P.O. Widlund, A. Pozniakovsky, E. Zanin, S. Bahmanyar, et al. 2015. Centrosomes. Regulated assembly of a supramolecular centrosome scaffold in vitro. *Science*. 348:808–812. <https://doi.org/10.1126/science.aaa3923>
- Xu, H., L.A. Sepúlveda, L. Figard, A.M. Sokac, and I. Golding. 2015. Combining protein and mRNA quantification to decipher transcriptional regulation. *Nat. Methods*. 12:739–742. <https://doi.org/10.1038/nmeth.3446>
- Zhang, Y.Q., A.M. Bailey, H.J. Matthies, R.B. Renden, M.A. Smith, S.D. Speese, G.M. Rubin, and K. Broadie. 2001. *Drosophila* fragile X-related gene regulates the MAP1B homolog Futsch to control synaptic structure and function. *Cell*. 107:591–603. [https://doi.org/10.1016/S0092-8674\(01\)00589-X](https://doi.org/10.1016/S0092-8674(01)00589-X)
- Zwicker, D., M. Decker, S. Jaensch, A.A. Hyman, and F. Jülicher. 2014. Centrosomes are autocatalytic droplets of pericentriolar material organized by centrioles. *Proc. Natl. Acad. Sci. USA*. 111:E2636–E2645. <https://doi.org/10.1073/pnas.1404855111>

Supplemental material

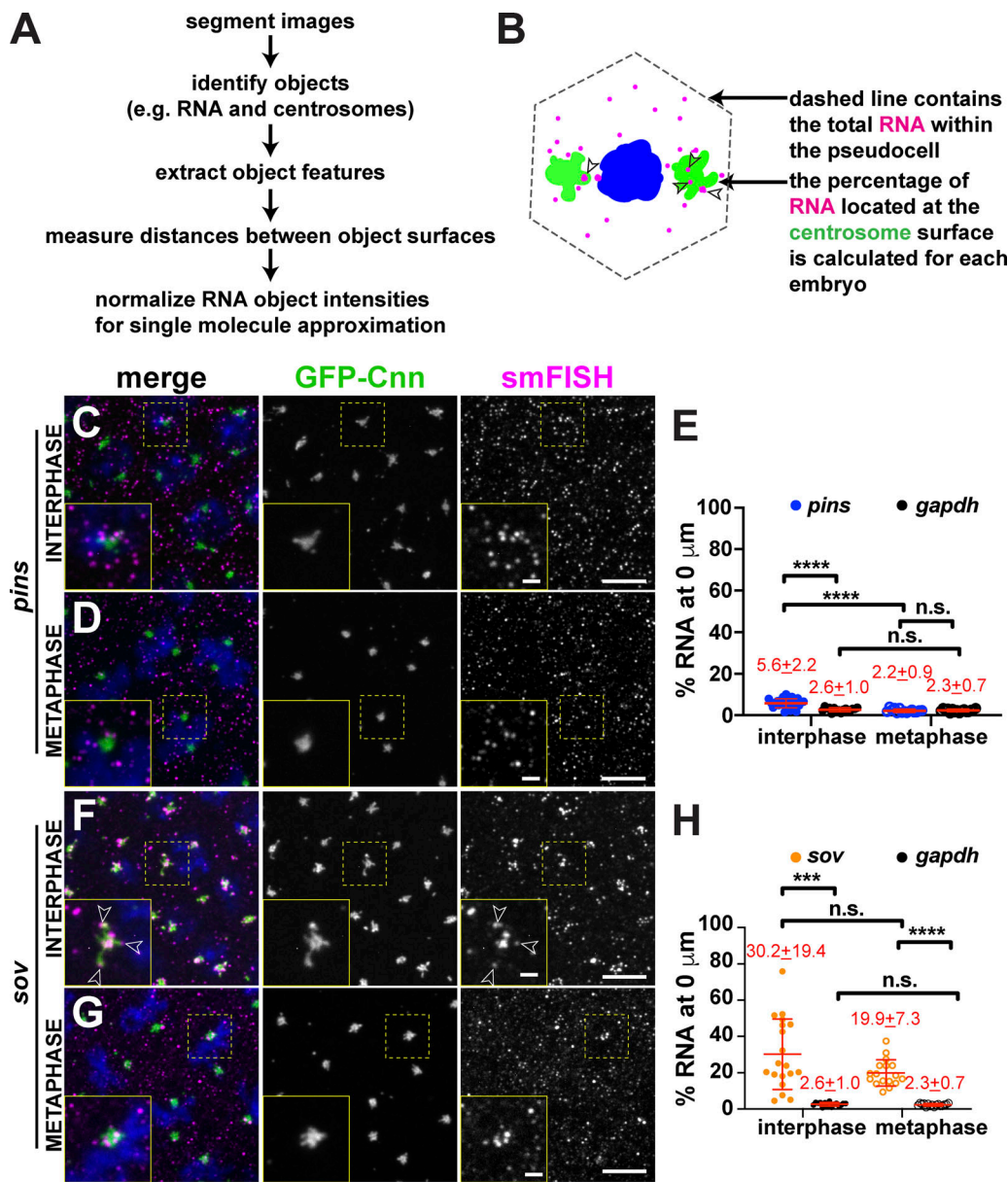


Figure S1. **Determining mRNA enrichment at centrosomes.** (A) Workflow used to quantify RNA distributions relative to centrosomes. (B) Cartoon shows total RNA (magenta) within a syncytial *Drosophila* embryo pseudocell (dashed line). Arrowheads show RNA overlapping with the centrosome (green) surface. (C–H) Maximum-intensity projections and quantification of smFISH for *pins* or *sov* mRNAs (magenta) in interphase and metaphase NC 13 embryos expressing GFP-Cnn (green). Boxed regions are enlarged in the insets. Open arrowheads denote association of *sov* mRNA with centrosome flares. Quantification of the percentage of RNA overlapping with the centrosome surface (0 μm distance) is shown to the right, where each dot represents a single measurement from $n = 16$ interphase and metaphase (*gapdh* mRNA), $n = 24$ interphase and 15 metaphase (*pins* mRNA), and $n = 19$ interphase and 17 metaphase (*sov* mRNA) embryos. Mean \pm SD are shown (red text). (C–H) *pins* (C–E) and *sov* (F–H). Note that values for *gapdh* are reproduced from Fig. 1 C to facilitate comparison. Table 1 lists the number of embryos, centrosomes, and RNA objects quantified per condition. ***, $P < 0.001$; and ****, $P < 0.0001$ by ANOVA followed by Dunnett’s T3 multiple comparisons test. Scale bars: 5 μm ; 1 μm (insets). n.s., not significant.

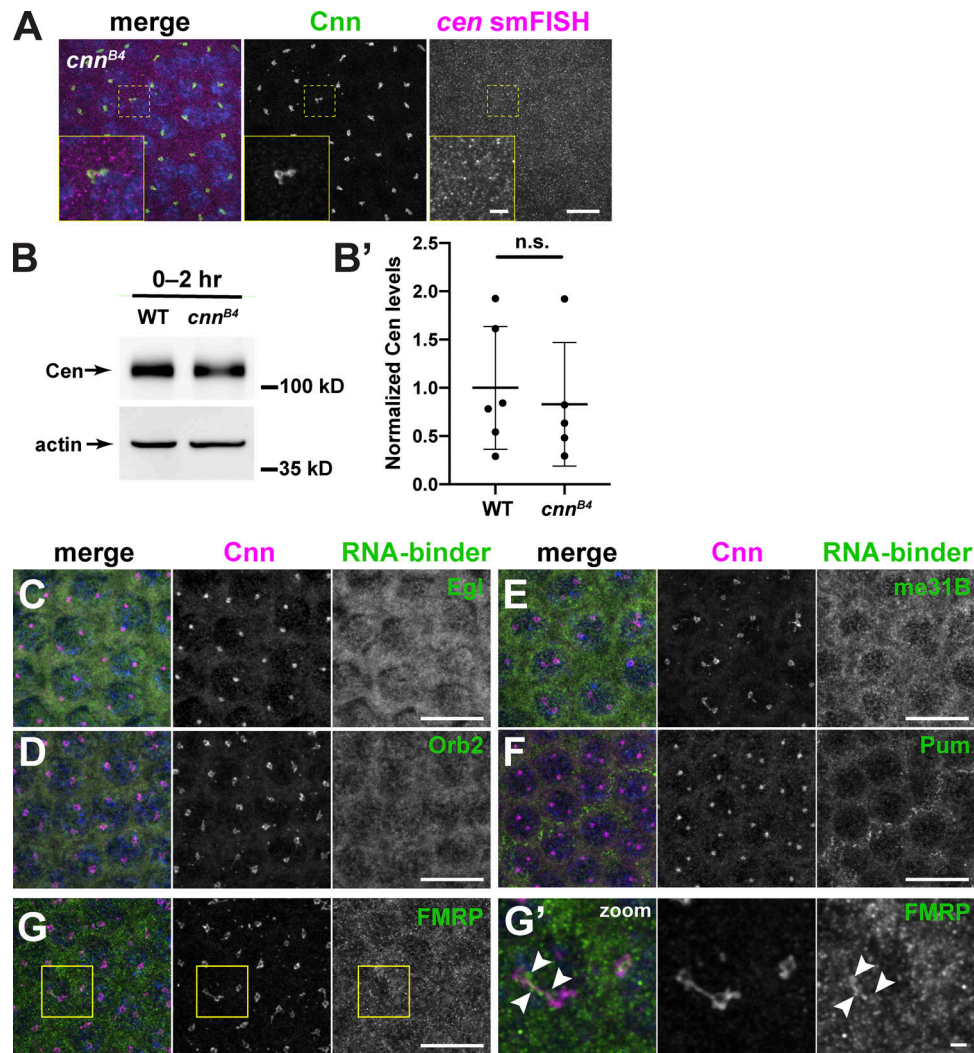


Figure S2. ***cen* mRNA granule formation requires the centrosome scaffold.** (A) Image shows immunofluorescence for Cnn (green) and *cen* smFISH (magenta) in an NC 12 *cnn*^{B4} embryo. Boxed region is enlarged in inset. Note the absence of large pericentrosomal *cen* mRNA granules. (B) Immunoblots show Cen protein content in 0-2-h (up to NC 14) WT and *cnn*^{B4} lysates. Actin is used as a loading control. (B') Each dot represents the levels of Cen normalized to the mean relative expression of the actin load control. n.s., not significant ($P = 0.672$) by unpaired *t* test from $n = 3$ independent biological replicates, with $n = 2$ technical replicates run on the same gel. (C-G') Images show interphase NC 12 embryos stained for Cnn (magenta) and antibodies for the indicated RNA-binding proteins (RNA-binder, green): Egl (C), Orb2 (D), me31B (E), Pum (F), and FMRP (G). (G') Inset from G; arrowheads, FMRP overlapping with Cnn. Scale bars: 10 μ m; 2 μ m (insets).

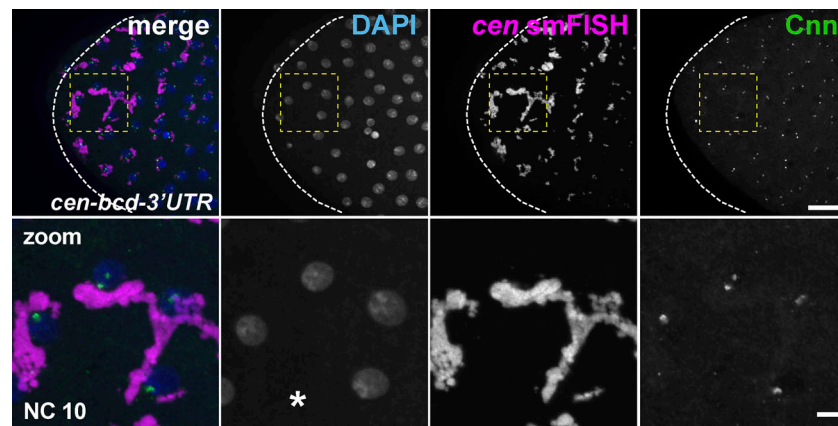


Figure S3. **Deregulation of *cen* mRNA granule formation.** (A) Immunoblots show Cen protein content relative to the actin loading control from 1–3-h embryonic extracts and are quantified in A'. Levels of Cen were normalized to the mean WT levels of actin from $n = 3$ independent biological replicates, each with $n = 2$ technical replicates run on the same gel. (B) Maximum-intensity projection of an interphase NC 10 embryo for *cen* mRNA labeled by smFISH (magenta), DAPI (nuclei, blue), and Cnn showing large *cen* RNPs. Asterisk marks nuclear fallout. Boxed regions enlarged below (zoom). Scale bars: 10 μm ; 2 μm (insets).

Provided online is one table. Table S1 lists all smFISH probes used in this study.